INFORMATION ENCODING ON A PSEUDO RANDOM NOISE RADAR WAVEFORM

THESIS

Joshua A. Hardin, Captain, USAF

AFIT-ENG-13-M-22

DEPARTMENT OF THE AIR FORCE
AIR UNIVERSITY

AIR FORCE INSTITUTE OF TECHNOLOGY

Wright-Patterson Air Force Base, Ohio

AFIT-ENG-13-M-22

INFORMATION ENCODING ON A PSEUDO RANDOM NOISE RADAR WAVEFORM

THESIS

Presented to the Faculty

Department of Electrical and Computer Engineering

Graduate School of Engineering and Management

Air Force Institute of Technology

Air University

Air Education and Training Command

in Partial Fulfillment of the Requirements for the

Degree of Master of Science in Electrical Engineering

Joshua A. Hardin, B.S.E.E.

Captain, USAF

March 2013

AFIT-ENG-13-M-22

INFORMATION ENCODING ON A PSEUDO RANDOM NOISE RADAR

WAVEFORM

Joshua A. Hardin, B.S.E.E.
Captain, USAF

Approved:

Peter J. Collins, PhD (Chairman)	19 FEB 2013 Date
Lt Col Geoffrey A. Akers, PhD (Member)	19 Feb 13 Date
Michael A. Temple, PhD (Member)	19 Feb 2013 Date

AFIT-ENG-13-M-22

Abstract

Navigation requires knowledge of current location and a planned destination. This is true with manned vehicles and unmanned vehicles. There are many ways to acquire the current location, including global positioning system (GPS), triangulation, radar, and dead reckoning. Today GPS is the most reliable and accurate navigation technique when there is a clear, unobstructed view of the satellite constellation. When there is an obstruction of the GPS satellite constellation, such as foliage or the roof of a building, navigation must be accomplished by other means. Various sensors can be used to perform indoor navigation; however, when the vehicle is autonomous the sensors need to provide the exact location to the system. This is where Random Noise Radars (RNRs) can fill a capability gap in indoor navigation. Because noise radar waveforms appear as white Gaussian noise (WGN), they do not generally interfere with other systems that may be operating in the vicinity.

This research determined if using a template replay strategy has the same RNR performance as using an analog noise source. Using the template replay approach, each RNR node has a priori knowledge about the transmitted waveforms of other nodes. Furthermore, when the template replay approach is used, it might be possible to communicate with other RNR platforms by creatively selecting the order in which templates are replayed.

The analysis here revealed that modifications do not significantly alter RNR functionality. Additionally, that template replay strategy was not detectable at signal-to-noise plus interference ratios (SNIRs) below -24 dB. The analysis revealed that even at SNIR equal to 0 dB, there are no parameters that can be reliably extracted other than transmitted signal bandwidth and transmitted template length; the transmitted message length was able to be extracted because the message was repeated over and over. If the message was not replayed the analysis showed that there would be no ability to extract

parameters. Finally, by using the RNR to transmit digitally generated templates, digital communication is possible and the symbol error rate (SER) is traceable to simulated SER.

Acknowledgments

I would like to first thank my wife who after finding out we were coming back to Dayton, Ohio did not ask for orders elsewhere. The support and encouragement I received from her helped me reach an accomplishment I really never thought would happen. I would also like to thank my parents who always knew that I would make it through all my schooling, even though there were times they thought that I had really endangered my education. Finally, I would like to thank my advisor for his time and patience.

Joshua A. Hardin

Table of Contents

Page

List of Figures

Figure Page

Figure Page

List of Tables

List of Acronyms

Acronym	Definition
ADC	analog to digital converter
AFIT	Air Force Institute of Technology
ALPINE	AFIT LORE Processing INtegrated Environment
ANT	Advanced Navigation Technology
ASCII	American Standard Code for Information Interchange
AUT	antenna under test
AWG	arbitrary waveform generator
AWGN	additive white Gaussian noise
BPSK	binary phase shift keying
CDMA	code division multiple access
DFSM	direct frequency-smoothing method
EM	electromagnetic
FAM	FFT accumulation method
FOPEN	foliage penetration
FPGA	field programmable gate array
GPS	global positioning system
GUI	graphical user interface
IRA	impulse radiating antenna
ISAR	inverse synthetic aperture radar (SAR)
LAN	local area network
LNA	low noise amplifier
LPA	log periodic antenna
LPD	low probability of detection

Acronym	Definition
LPI	low probability of intercept
LTI	linear time invariant
NTR	noise technology radar
OFDM	orthogonal frequency-division multiplexing
PCB	printed circuit board
PCI	Peripheral Component Interconnect
PSD	power spectral density
QMF	quadrature mirror filter
QMFB	quadrature mirror filter bank
RAIL	Radar Instrumentation Laboratory
RCS	radar cross-section
RF	radio frequency
RNR	random noise radar
RSR	random signal radar
SAR	synthetic aperture radar
SCD	spectral correlation density
SDR	software defined radio
SER	symbol error rate
SNIR	signal-to-noise plus interference ratio
SNR	signal-to-noise ratio
TTL	transistor-transistor logic
UAV	unmanned aerial vehicle
UWB	ultrawideband
VLSI	very large scale integration
WGN	white Gaussian noise

Acronym	Definition
WSS	wide sense stationary

INFORMATION ENCODING ON A PSEUDO RANDOM NOISE RADAR WAVEFORM

I. Introduction

1.1 Problem Description

Navigation requires knowledge of current location and a planned destination. This is true with manned vehicles and unmanned vehicles. There are many ways to acquire the current location, including global positioning system (GPS), triangulation, radar, and dead reckoning. Today GPS is the most reliable and accurate navigation technique when there is a clear, unobstructed view of the satellite constellation. When there is an obstruction of the GPS satellite constellation, such as foliage or the roof of a building, navigation must be accomplished by other means. Various sensors can be used to perform navigation indoors; however, when the vehicle is autonomous the sensors need to provide the exact location to the system. This is where noise radar can fill a capability gap in indoor navigation. Because noise radar is white Gaussian noise (WGN), it will not interfere with other systems that may be operating in the vicinity.

To perform navigation using the Air Force Institute of Technology (AFIT) random noise radar (RNR), the radar system needs to be set up in a multistatic mode where there are at least 3 radar nodes and one target. The AFIT RNR currently performs multistatic operation by sampling the outgoing radar signal and passing the sampled transmission to all the other nodes over a wireless or wired ethernet connection. Implementing a template replay approach where the template bank is stored on each of the nodes will facilitate the multistatic operation of the AFIT RNR without relying on a wireless or wired Ethernet connection.

This research will determine if using a template replay strategy has the same radar performance as using an analog noise source. Using the template replay approach, each node will have a priori knowledge about the waveforms for the other nodes. Furthermore, if the template replay approach is used, it might be possible to communicate with other RNR platforms by creatively selecting the order in which templates are replayed.

1.2 Research Motivation

Autonomous navigation is a major part of the development of autonomous vehicles in the Department of Defense. Having capability for micro unmanned aerial vehicles (UAVs) to operate in an indoor environment is key for several different scenarios including intelligence gathering, clearing a building, or search and rescue. From a military perspective being able to perform these kinds of missions without detection or interruption is advantageous. Because the AFIT RNR is low power and is an ultrawideband (UWB) waveform, the probability of detection is low. The noise generated is WGN, which will only correlate with an exact replica of the original waveform; therefore, the AFIT RNR has the classification of low probability of detection (LPD) and a low probability of intercept (LPI) radar. Additionally, the low power requirements of the RNR may allow for a small, compact, rapidly deployable capability.

1.3 Research Goals

The overall goal of this research is to continue developing and improving the AFIT RNR. This research will primarily focus on the following objectives:

1. develop and implement a completely digital UWB RNR,
2. characterize the developed system and compare it to the current system,
3. develop a process by which the template replay approach can be used for multistatic radar, and

4. demonstrate the ability to perform simultaneous radar and communication.

The secondary objectives include, but are not limited to:

1. improve the digital software processing of the current AFIT RNR by using the template replay approach, and

2. enhance the AFIT NoNET software.

1.4 Background

The idea of using noise as a radar waveform first started around 1904, when Christian Huelsmeyer first used noise pulses in his "telemobiloscope." Radars that use noise as the waveform have been referred to as noise technology radar (NTR), RNR, or random signal radar (RSR). In 1959, B.M. Horton introduced the use of correlation with the noise waveform for use in distance measuring equipment. Horton discusses how the noise waveform makes the average output of the system an unambiguous function of distance [6]. For approximately 40 years, little research was accomplished in the area of noise radar. The lack of interest in RNR was primarily because signal generation techniques were immature. Now with the use of very large scale integration (VLSI) and solid state devices, research is becoming more prevalent [5]. Current technology is driving field programmable gate arrays (FPGAs) and arbitrary waveform generators (AWGs) to become main devices in implementing noise radars. This is because the FPGA has the ability to correlate very fast and the AWG has the ability to generate any waveform that is programmed and loaded into its memory. Noise radars fill important capability gaps within military systems, such as LPI, LPD, and anti-jam [11]. Coherent noise radars usually provide simplified designs while preserving the advantages of traditional radar systems [16]. Various applications for noise radar include radar cross-section (RCS) measurements, Doppler estimation, ground penetrating radar, synthetic aperture radar (SAR), inverse SAR (ISAR), and foliage penetration (FOPEN) [16].

The idea of using a radar or communication system in a dual role capability is an idea that piqued the interests of both the military and car manufacturers [7] [15]. Current research thrusts for joint radar and communication systems are focused on the orthogonal frequency-division multiplexing (OFDM) and code division multiple access (CDMA) waveforms. The Ohio State University has demonstrated a simultaneous radar and communication system using an OFDM waveform in a software defined radio (SDR) [21]. The Ohio State University's SDR was able to transmit the range-Doppler map from the previously transmitted pulses. Their system was able to obtain a peak communication rate of 150 Mbps.

Over the last few years, AFIT has developed its own RNR. AFIT's RNR is based on a Pennsylvania State University design, which uses an analog noise source to produce the noise signal. Schmitt started the first effort at AFIT, where she studied the concept of through the wall imaging [22]. Next, Nelms introduced multiple nodes and full utilization of multistatic channels to increase the cross-range resolution and accuracy of the AFIT RNR [17]. Since then, several students have worked on improving the AFIT RNR. Priestly briefly investigated the template replay strategy. His qualitative assessment was the level of covertness could be maintained, provided that the play back of the templates did not have a obvious periodicity [19]. Thorson improved the time to perform Doppler processing from about 40 minutes to less than two minutes [23]. This research will enhance the AFIT RNR by providing the capability to perform radar, communication, or navigation using any digitally generated waveform. Additionally, this research will show how radar parameters might be extracted and estimated using a set of LPI parameter estimation tools.

1.5 Organization of Thesis

Further discussions of the principles of the AFIT RNR and the theory needed to develop predictions and compare results are found in Chapter 2. In Chapter 3, the simulation and experimental methodology used in this research effort are presented. A detailed analysis of the results along with a performance and utility assessment is provided in Chapter 4. The conclusions and recommendations for future research are discussed in Chapter 5.

II. Theory

2.1 Chapter Overview

This chapter explains the theory that is needed to perform the experiments and analyze the results associated with implementing simultaneous communications and radar in the Air Force Institute of Technology (AFIT) random noise radar (RNR). First, correlation receiver theory will be discussed. The AFIT RNR uses a correlation receiver to separate the transmitted noise signal from the interference. Then theory pertaining to general radar principles will be discussed. This system is focused on performing radar as the primary mission and communication as the secondary mission. Therefore, radar theory will be used to determine communication parameters. Next, low probability of intercept (LPI) theory will be discussed and techniques for evaluating LPI signals will be introduced and explained. LPI theory is necessary to ensure that the modifications made to the current system do not impact the covertness that is inherent in a noise radar.

2.2 RNR Theory

There are several different configurations of a noise radar receiver. The most common configuration is the correlation receiver. The correlation receiver uses the correlation function, which is defined as

$$R_X(t_1, t_2) = E\left[X(t_1)X^*(t_2)\right] \tag{2.1}$$

$$= \int_{-\infty}^{\infty} X(t_1)X^*(t_2)dt \tag{2.2}$$

where $E[]$ is the expected value of a function and where $X(t)$ is an arbitrary random function. Other types of radar receivers used with noise radars include the spectrum analysis receiver and the anticorrelation receiver. The spectrum analysis receiver uses spectrum analysis after mixing the transmitted signal with the received signal. By mixing

the transmitted with received signal a motionless target will produce a periodic modulation. This modulation can be used is directly proportional to the distance between the target and antenna [5]. The anticorrelation receiver was first introduced by Horton [6]. The anticorrelation receiver uses the anticorrelation function, which is $H(\tau) = 1 - R(\tau)$, to determine the distance between the target and the antenna. In the anticorrelation receiver the noise signal is frequency modulated. The mean instantenous modulated frequency is given as

$$\overline{\Delta W} = \sqrt{\frac{2}{\pi}\overline{\Delta W^2}} = A\sqrt{H(\tau)}, \tag{2.3}$$

where A is a constant to a specific white Gaussian noise (WGN) source. By directly measuring the mean or variance, $H(\tau)$ can be estimated [6]. Using a lookup table with experimentally derived $H(\tau)$ values, delay times τ can be determined. The results from Horton's experiment are seen in Figure 2.1.

2.2.1 Correlation Receiver Theory.

The AFIT RNR uses the correlation receiver implementation of a noise radar. Correlation receivers are based on the correlation implementation of a matched filter. A matched filter is the optimum filter given the following conditions exist:

1. additive white Gaussian noise (AWGN) is the only corruption present in the received signal,
2. the system is linear time invariant (LTI) and stable with impulse response h(t),
3. the transmitted signal has a constant power spectral density (PSD) or is wide sense stationary (WSS).

A signal is considered to be WSS if "the mean does not depend on time and average value of the product of two samples should only depend on the interval between the samples" [8]. The AFIT RNR is a WGN waveform, and therefore has a Gaussian distribution. The mean

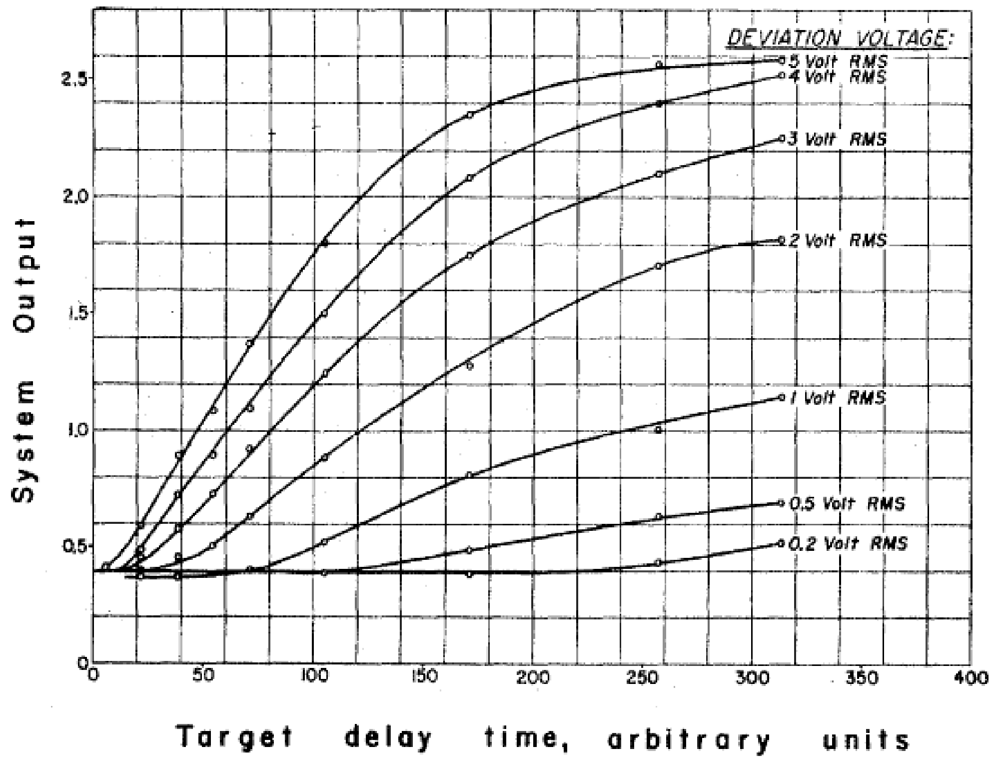

Figure 2.1: Performance of a simple noise modulated system [6]

or expected value of a Gaussian distribution is constant and zero for WGN. The second moment or the covariance is only dependent on the time difference. Specifically for WGN the covariance is 0 except when the time difference τ is equal to 0, where the covariance is 1. Mathematically WSS is defined as

$$\mu_X[n] = \mu \quad \text{(a constant)} \qquad -\infty < n < \infty \tag{2.4}$$

$$c_X[n_1, n_2] = g(|n_2 - n_1|) \qquad -\infty < n_1 < \infty, \quad -\infty < n_2 < \infty. \tag{2.5}$$

The AFIT RNR meets all the criteria above; therefore, the matched filter is the optimal filter. The algorithm for the matched filter is defined as

$$y_m(t) = \int_{-T}^{0} s_m(-\tau)x(t-\tau)d\tau \tag{2.6}$$

where y_m is the output of the filter, T is the duration of the input waveform $x(t)$, and s_m is the m^{th} signal to be tested [24].

An important property of noise radar is that a realization of WGN is uncorrelated in time with any other realization of WGN. However, when a realization of WGN is correlated with a scaled in amplitude version of itself that has been added with another realization of WGN, the correlation process will detect the realization of WGN in extremely high noise environments. Figure 2.2(a) shows the received signal in blue and then the delayed version of the transmitted signal overlaid in red for visual reference. Note that the transmitted signal is not visible to the eye when looking at the received signal. Figure 2.2(b) shows the correlation output with a peak that corresponds to the time delay. This property is the primary reason that correlation receivers are used in noise radar technology.

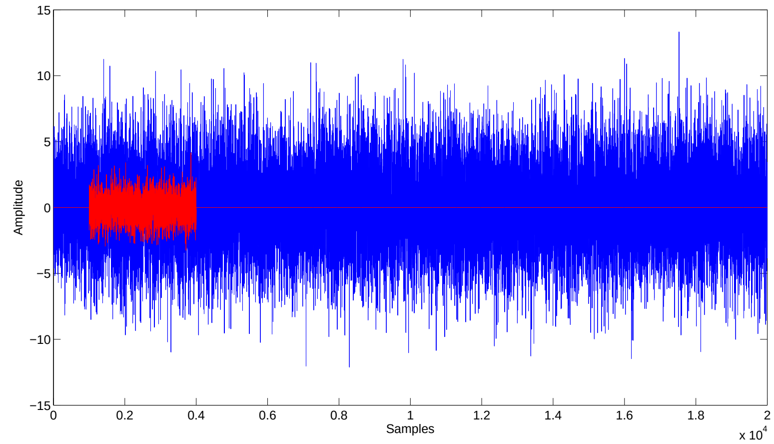

(a) Comparison of signal at SNR = ∞ (red) and SNR = -10 dB (blue)

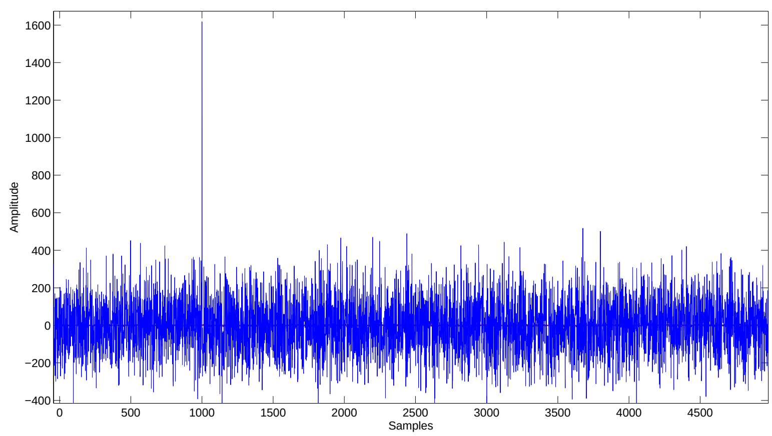

(b) Correlator output for an WGN pulse in a AWGN channel

Figure 2.2: Effectiveness of correlation for SNR = -10 dB

2.3 Radar Theory

Radar is defined as "an electrical system that transmits radio frequency (RF) electromagnetic (EM) waves toward a region of interest and receives and detects these EM waves when reflected from objects in that region" [20]. Figure 2.3 shows the major elements of a radar system.

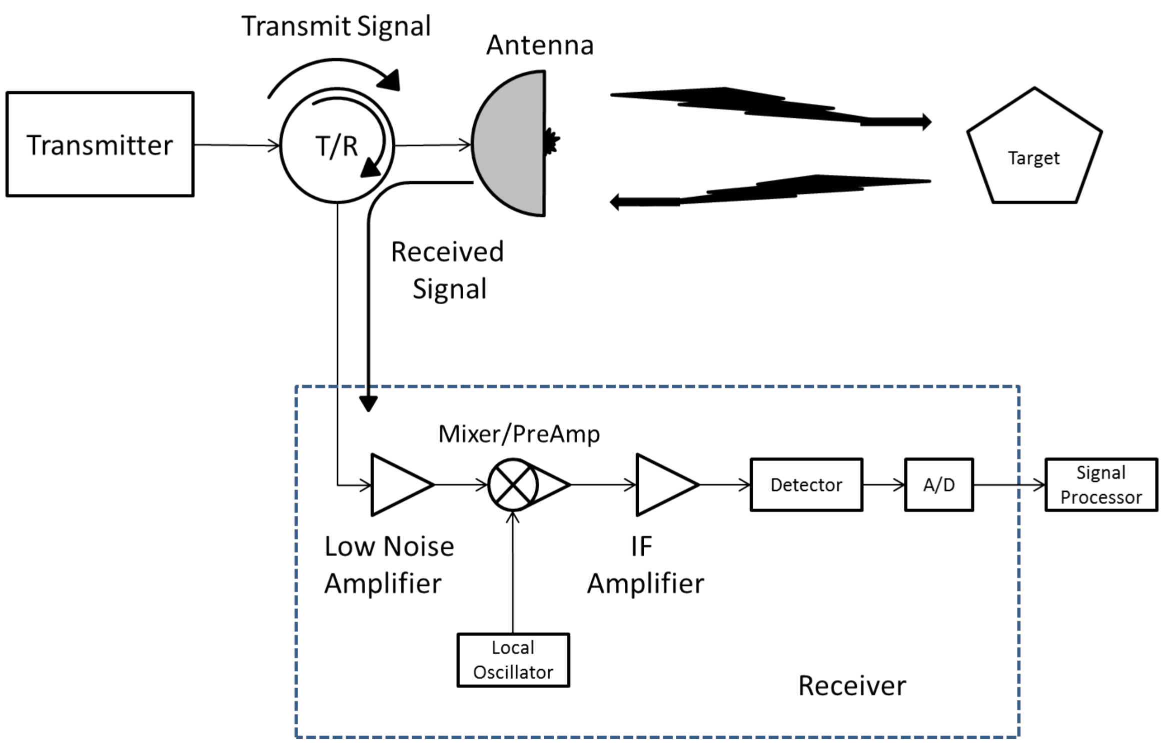

Figure 2.3: Basic monostatic radar diagram [20]

The power density incident (Q_i) on a target at a range (R) from an isotropic radiator is defined as [20] [9]

$$Q_i = \frac{P_t}{4\pi R^2} \tag{2.7}$$

where P_t is the radar total peak transmit power. In most radar systems, an antenna is employed that has a directional antenna pattern; therefore, an additional gain factor (G_t)

needs to be accounted for in determining the power at the target, resulting in

$$Q_i(\theta) = \frac{P_t G_t(\theta)}{4\pi R^2}. \tag{2.8}$$

The power reflected from the target back towards the radar is the amount of incident power density (Q_i) multiplied by a scaling factor (σ) known as radar cross-section (RCS) resulting in,

$$P_{refl}(\theta) = Q_i(\theta)\sigma = \frac{P_t G_t(\theta)\sigma}{4\pi R^2}. \tag{2.9}$$

RCS is a fictitious quantity that is similar to the antenna design concept of an effective area. The RCS of a target is a useful characteristic to determine and compare electrical effective areas. RCS can be determined using an instrumentation radar by using the following relationship,

$$\sigma = \lim_{R\to\infty} 4\pi R^2 \frac{|E_s|^2}{|E_i|^2}, \tag{2.10}$$

where E_s is the scattered field and E_i is the incident field [9]. The limiting process is applied so that the RCS measurements are taken in the far-field where the incident EM waves are approximately plane waves and so RCS is not a function of range.

The power reflected from the target propagates back towards the radar system and has a power density (Q_r) at the radar system of

$$Q_r = \frac{P_{refl}}{4\pi R^2}. \tag{2.11}$$

Combining Equations 2.9 & 2.11 results in

$$Q_r = \frac{P_t G_t \sigma}{(4\pi)^2 R^4}; \tag{2.12}$$

applying the effective area of the antenna (A_e) gives the power in watts received by the radar system,

$$P_r = Q_r A_e = \frac{P_t G_t A_e \sigma}{(4\pi)^2 R^4}. \tag{2.13}$$

Many times the gain of an antenna (G_t) will be represented in terms of the antenna's effective area and the wavelength of the antenna, resulting in the well known radar range equation [20]

$$P_r = \frac{P_t G_t \lambda^2 \sigma}{(4\pi)^3 R^4}. \tag{2.14}$$

As discussed in Section 2.2, the AFIT RNR uses a correlation receiver, and the correlation output has a peak when the received signal overlaps the transmitted signal. The time at which that peak occurs is round trip time. The range to the target can be determined by using the speed of light (c) and the time delayed (ΔT) ,

$$R = \frac{c\Delta T}{2}. \tag{2.15}$$

A useful characteristic of any radar system is the ability to resolve multiple targets. The minimum range that two targets can be distinguished is given by,

$$\Delta R = \frac{c}{2B} \tag{2.16}$$

where B is the instantaneous bandwidth of the radar system [20].

2.4 Power Estimation

Transmitted power can be estimated using the first and second moments, or the mean and variance, of the transmitted signal. The average power transmitted is given by Parseval's theorem,

$$P_{Av}^{T} \equiv \frac{1}{T}\int_{t_i}^{t_i+T} s^2(t)dt \approx \frac{1}{(N-1)\Delta t}\sum_{i=0}^{N-1} s^2(t_i)\cdot\Delta t = \frac{1}{N-1}\cdot\sum_{i=0}^{N-1} s^2(t_i). \tag{2.17}$$

Estimated mean and variance are given as [8]

$$\mu_s = \frac{1}{N-1}\sum_{i=0}^{N-1} s_i \tag{2.18}$$

$$\sigma^2 = \frac{1}{N-1}\sum_{i=0}^{N-1}(s_i - \mu_s)^2. \tag{2.19}$$

To get to Equation 2.17 from the discrete variance,

$$\sigma^2 = \frac{1}{N-1}\sum_{i=0}^{N-1}(s_i - 2\mu_s s_i + \mu_s^2) = \frac{1}{N-1}\left\{\sum_{i=0}^{N-1} s_i^2 - \sum_{i=0}^{N-1} 2\mu_s s_i + \sum_{i=0}^{N-1}\mu_s^2\right\} \tag{2.20}$$

$$= \frac{1}{N-1}\sum_{i=0}^{N-1} s_i^2 - \frac{1}{N-1}\sum_{i=0}^{N-1} 2\mu_s s_i + \frac{1}{N-1}\sum_{i=0}^{N-1}\mu_s^2 \tag{2.21}$$

$$= \frac{1}{N-1}\sum_{i=0}^{N-1}\left(s_i^2 + \mu_s^2 - 2\mu_s \frac{1}{N-1}\sum_{i=0}^{N-1} s_i\right) \tag{2.22}$$

$$= \frac{1}{N-1}\sum_{i=0}^{N-1}\left(s_i^2 + \mu_s^2 - 2\mu_s^2\right) \tag{2.23}$$

$$= \frac{1}{N-1}\sum_{i=0}^{N-1}\left(s_i^2 - \mu_s^2\right). \tag{2.24}$$

Therefore, adding in μ_s^2 will yield an estimate of average transmitted power,

$$P_{Av}^T \approx \sigma_s^2 + \mu_s^2 = \frac{1}{N-1}\sum_{i=0}^{N-1} s_i^2 \tag{2.25}$$

2.5 LPI Theory

Although there is no formal ANSI/IEEE definition of LPI, Phillip Pace offers the following definition [18]: "A low probability of intercept (LPI) radar is defined as a radar that uses a special emitted waveform intended to prevent a non-cooperative intercept receiver from intercepting and detecting the emission."

There are many military applications for radars with LPI properties. These applications include altimeters, landing systems, airborne radar, and missile seekers [18]. This section will cover three types of exploitation techniques commonly used to detect or intercept radar parameters. These techniques are autocorrelation, quadrature mirror filter banks (QMFBs), and cyclostationary spectral analysis.

2.5.1 Autocorrelation.

The autocorrelation technique uses the correlation function to determine if there are any repeating elements within a captured signal. The autocorrelation,

$$R_X(t_1, t_2) = E\left[X(t_1)X^*(t_2)\right] \tag{2.26}$$

$$= \int_{-\infty}^{\infty}\int_{-\infty}^{\infty} X(t_1)X^*(t_2) f_{X(t_1),X^*(t_2)}\left(X(t_1), X^*(t_2)\right) dX(t_1)dX(t_2) \tag{2.27}$$

is the expected value of a single signal of interest multiplied by the signal of interest's complex conjugate at a different time.

Figure 2.4 shows the autocorrelation of a sinusoidal signal. The X-axis is the amount of time that one signal lags another in the correlation process. At zero-lag the signal and the complex conjugate are completely overlapped, and there is a maximum for the autocorrelation function. Positive autocorrelation peak amplitudes represent times where the signal is repeated.

Figure 2.5 is an illustration where the signal leads (positive lag) the complex conjugate. Negative autocorrelation peaks are where the signal and the complex conjugate are 180° out of phase.

2.5.2 Quadrature Mirror Filter Bank.

The QMFB uses wavelet filters to break a signal down into several time-frequency layers. By analyzing the layers, signal parameters of LPI signals can be determined. These parameters are bandwidth, center frequency, energy distribution, phase modulation, signal duration, and location in the time-frequency plane [18]. Wavelets are wavelike functions that map the signal of interest into another plane, which would be more useful for processing. In other words, a wavelet is a time limited bandpass filter when wavelets are used in signal processing [1]. A quadrature mirror filter (QMF) consists of an iteration of filter pairs to generate the wavelets. By varying the window resolution, time resolution can

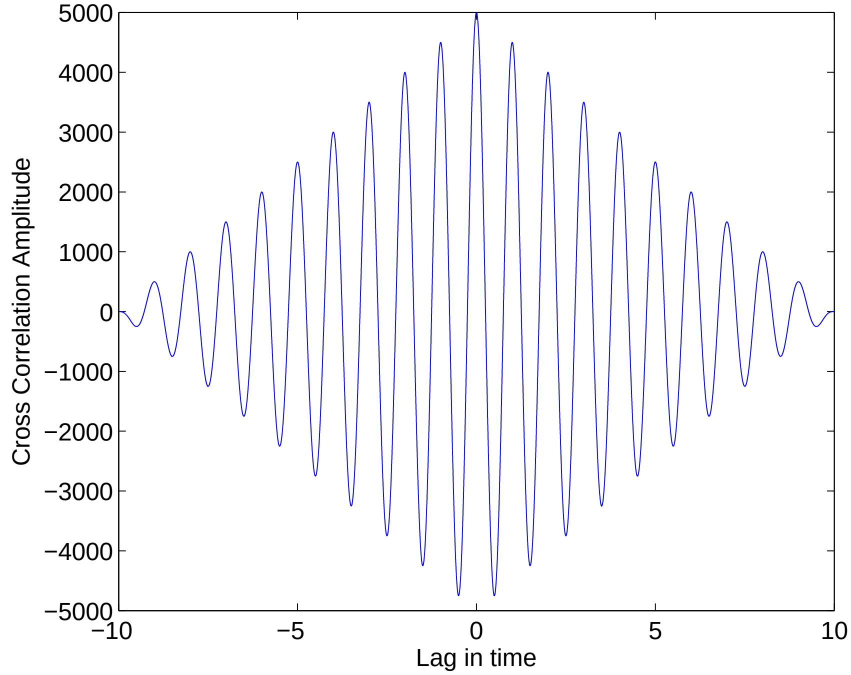

Figure 2.4: Autocorrelation of a sinusoidal signal

be sacrificed for resolution in frequency. The filter bank is a set of filters that separate the input signal into frequency bands that can be manipulated more efficiently than the original signal [18]. A diagram of a QMFB tree is shown in Figure 2.6, where G and H represent high and low pass filters. Each filter block in Figure 2.6 represents a wavelet using the basis function and prototype wavelet $h(t)$,

$$h_{a,b}(t) = \frac{1}{\sqrt{a}} h\left(\frac{t-b}{a}\right). \tag{2.28}$$

For large values of a, the basis function is a stretched version of the prototype wavelet. For small values of a, the basis function is a compressed version of the prototype wavelet. A popular prototype wavelet is the sinc filter. Pace describes the sinc wavelet filter as [18]

$$h(n) = \frac{1}{\sqrt{2}} sinc\left(\frac{n+0.5}{2}\right). \tag{2.29}$$

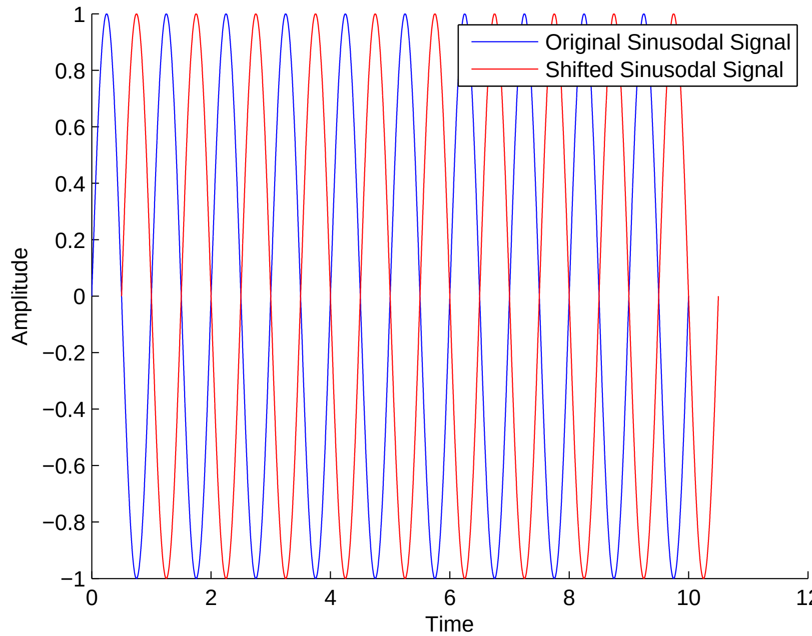

Figure 2.5: Sinusoidal signal and a sinusoidal signal shifted by 180°

There are an infinite number of coefficients of the sinc wavelet filter. If the filter is truncated a small amount of non-orthogonality with in the filter coefficients, cross correlation, and Gibbs phenomena (that occurs with a rectangular window) will occur. A hamming window is often used to mitigate the Gibbs phenomena. By using a Hamming window, energy is lost due to the loss of orthogonality when truncating the filter. Trading off a small amount of cross correlation between filters for more energy in each tile can be accomplished by having a passband greater than $\pi/2$. Additionally, it is desirable to rescale the coefficients so the sum of the squares are equal to one. Making the above modifications to the sinc filter results in the modified sinc filter,

$$h(n) = \sqrt{\frac{S}{2}} sinc\left(\frac{n + 0.5}{C}\right) w(n) \tag{2.30}$$

where C is the compression variable, S is the scaling variable, and $w(n)$ is the Hamming window used to suppress Gibbs phenomena [18].

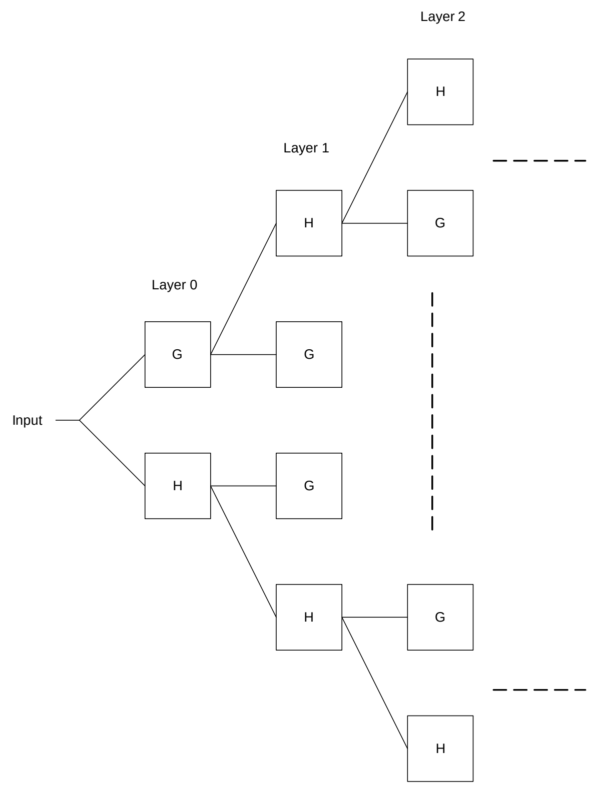

Figure 2.6: A QMFB tree diagram [18]

To understand the signal analysis using a QMFB, a seven bit barker code with a binary phase shift keying (BPSK) signal was used as a test signal. This signal is put through the QMFB code provided by Pace and analyzed at several layers [18]. Consider layer three, shown in Figure 2.7. This layer provides some resolution in the frequency direction but has very good resolution in the time direction. By having very good resolution in the time dimension, the number of periods that were captured can be determined. By counting the number of peaks, one can determine the number of periods captured in the test signal; the 7-bit Barker code was repeated 25 times.

The next layer to look at is a layer in the middle where there is balance in time and frequency resolution. Using the color plot of layer 6 shown in Figure 2.8, the bandwidth can be determined. In Figure 2.8 the bandwidth is determined to be 1 kHz.

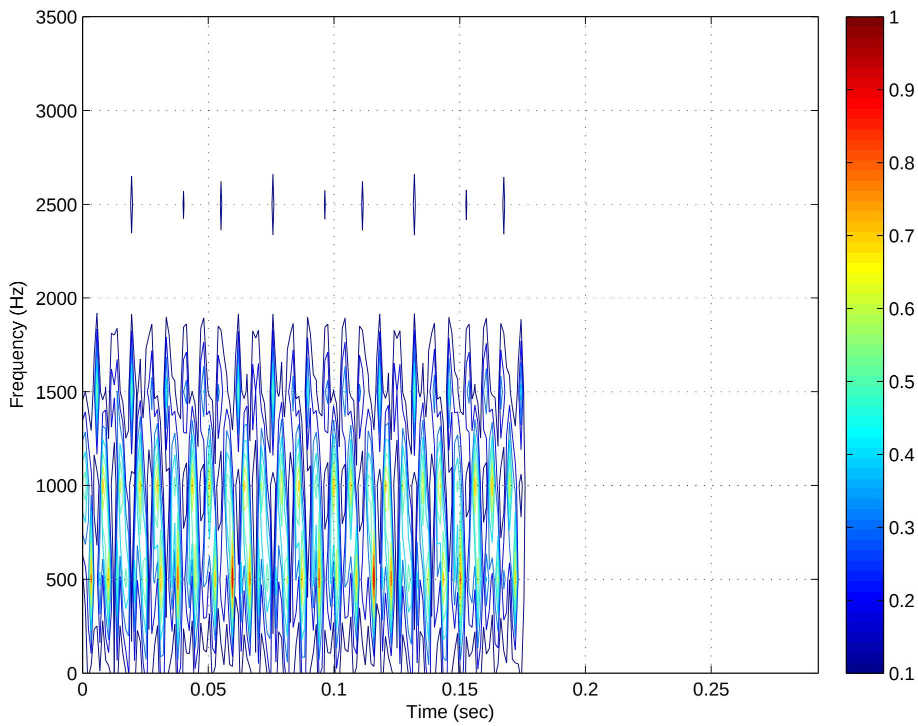

Figure 2.7: QMFB layer 3 *contour plot* for 7-bit barker code BPSK test signal

2.5.3 Cyclostationary Spectral Analysis.

Where the autocorrelation analysis technique in Section 2.5.1 models the signal of interest as a stationary process, the cyclostationary spectral analysis technique models the signal of interest as a cyclostationary process. A signal is considered to be cyclostationary of order n if and only if an nth order nonlinear transformation of the signal will create sine wave components that result in distinct lines in frequency spectrum [18]. Signals that are stationary will only have a spectral line at zero. Modeling the signal as a cyclostationary process provides advantages for LPI radar parameter estimation by using the nonzero correlation between frequency components when their frequency of separation is related to the periodicity of interest [18].

The QMFB analysis is a good technique for determining time-frequency results that allow for good estimation of LPI parameters. The cyclostationary technique transforms

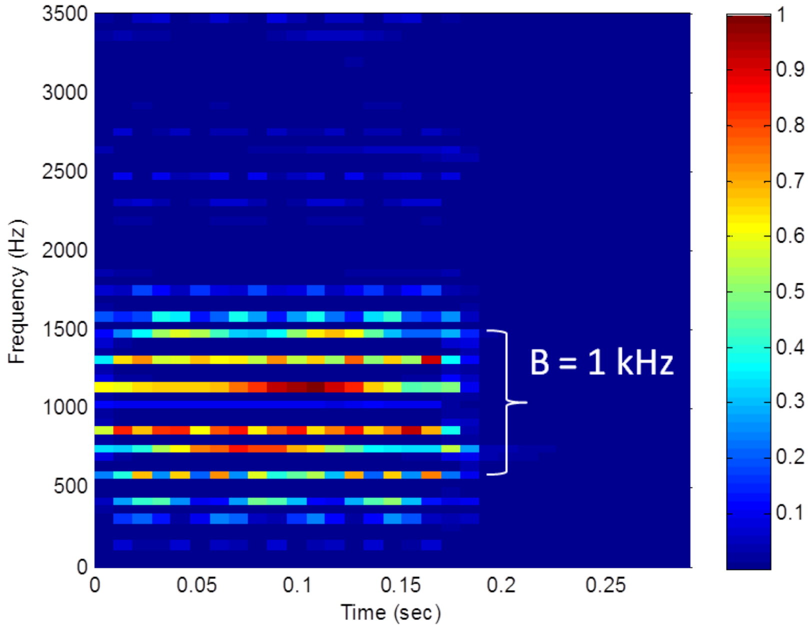

Figure 2.8: QMFB layer 6 *color plot* for 7-bit barker code BPSK test signal

time domain signals into frequency-cycle frequency domain that adds capability for detection and classification of LPI signals. The cyclic autocorrelation function and the spectral correlation density form the basis of the cyclostationary technique for LPI parameter extraction.

The cyclic autocorrelation function of a complex-value time series signal $x(t)$ is defined by [4]

$$R_x^{\alpha}(\tau) \triangleq \lim_{T\to\infty} \frac{1}{T} \int_{-T\backslash 2}^{T\backslash 2} x\left(t+\frac{\tau}{2}\right) x^*\left(t-\frac{\tau}{2}\right) e^{-j2\pi\alpha t} dt. \tag{2.31}$$

The signal $x(t)$ is said to be cyclostationary if $R_x^{\alpha}(\tau)$ is not zero at delay τ and cycle frequency $\alpha \neq 0$. Recalling from random signal analysis theory, the power spectral density is defined as the Fourier transform of the autocorrelation function. Similarly, the spectral correlation density (SCD) is defined as the Fourier transform of the cyclic autocorrelation function [4]

$$S_x^{\alpha}(f) = \int_{-\infty}^{\infty} R_x^{\alpha}(\tau) e^{-j2\pi\alpha\tau} d\tau = \lim_{T\to\infty} \frac{1}{T} \int_{-T\ 2}^{T\ 2} X_T\left(t+\frac{\alpha}{2}\right) X_T^*\left(t-\frac{\alpha}{2}\right) \tag{2.32}$$

where α is the cyclic frequency, leading to the two dimensional bifrequency plane. Equations 2.31 and 2.32 represent the basis of the cyclostationary spectral analysis.

There are computationally efficient algorithms used to estimate the SCD. These algorithms are the FFT accumulation method (FAM) and direct frequency-smoothing method (DFSM). The FAM algorithm divides the bifrequency plane into smaller portions and calculates one region at a time using the FFT. A block diagram of the FAM algorithm is shown in Figure 2.9. The block diagram of the DFSM algorithm is shown in Figure 2.10. The DFSM algorithm is less efficient than the FAM algorithm but is easier to implement [18].

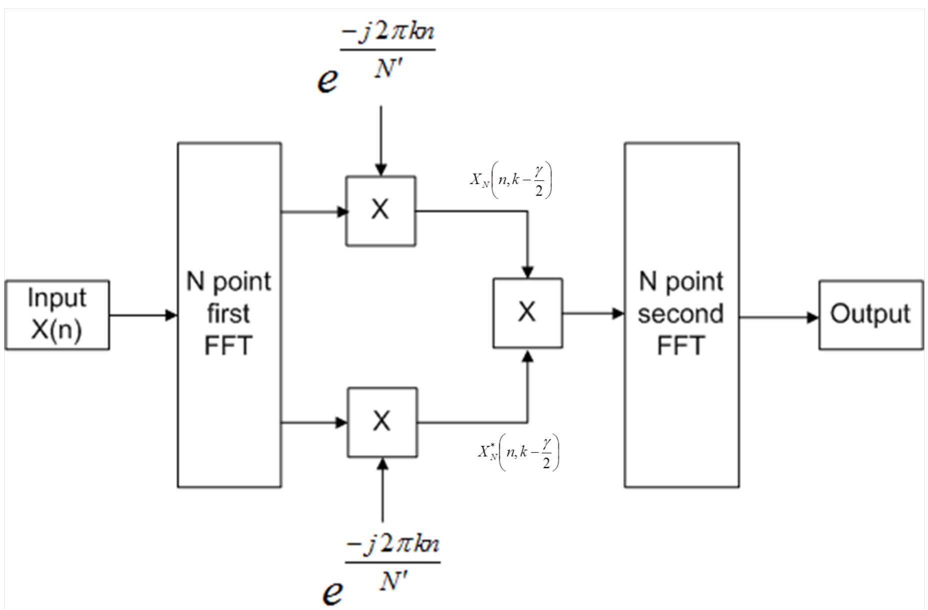

Figure 2.9: Block diagram of the FAM time smoothing method to estimate the SCD

To illustrate how parameters are extracted from a signal, a seven-bit BPSK signal is used as a test signal. The test signal has a bandwidth of $1kHz$ and is modulated using the Barker code. Figure 2.11 shows the entire SCD using the DFSM to perform the cyclostationary spectral analysis. Notice there are four quadrants where the BPSK signal

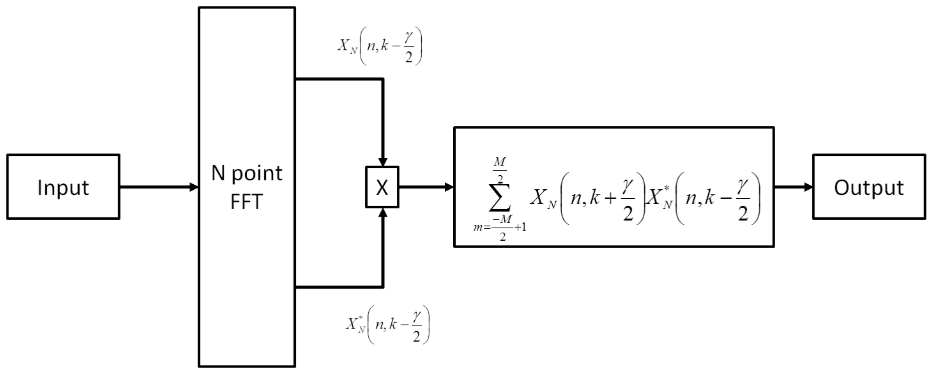

Figure 2.10: Block diagram of the DFSM direct frequency-smoothing algorithm to estimate the SCD

shows up. The SCD is bounded in the frequency direction by $-f_s/2$ to $f_s/2$, and the cycle frequency is bounded by $-f_s$ to f_s.

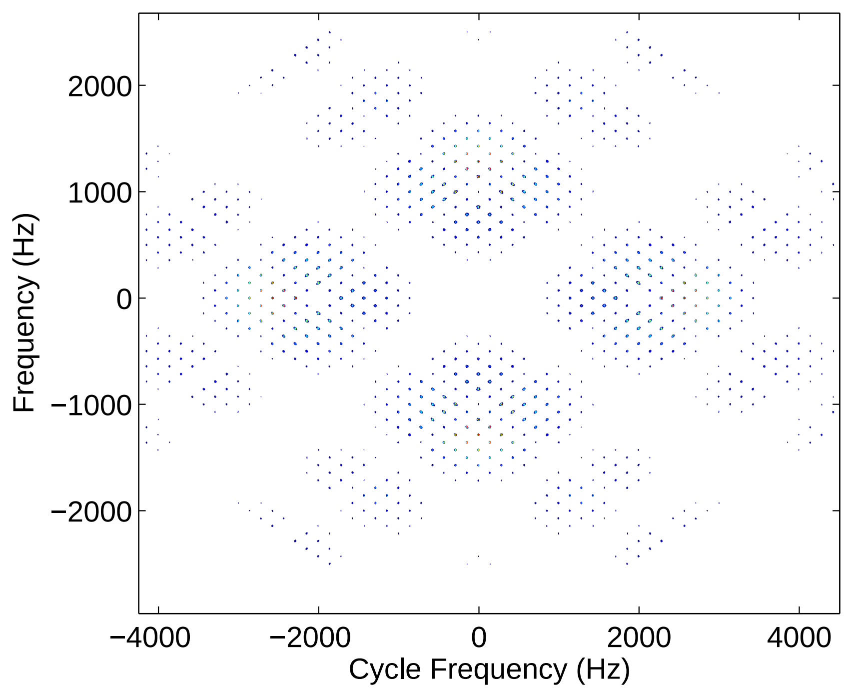

Figure 2.11: DFSM SCD of a 7-bit Barker code BPSK signal

A closer look at one quadrant will provide the necessary resolution to determine parameters of the test signal. Figure 2.12 shows the top quadrant. As annotated in Figure 2.12, the bandwidth can be determined by observing where the SCD peaks before falling off in amplitude. The region that the arrow points to is where the SCD falls off in amplitude. This is largely subjective when there is not a clear drop off in amplitude between the peaks. The bandwidth is found to be 1 kHz. By counting the number of peaks in the bandwidth, the number of bits used can be determined. If the peaks inside the region annotated by the arrow were to be counted, the number of bits and the bandwidth would be incorrect. By counting the number of peaks, the number of bits is 7. The rate at which the barker code is transmitted is found by measuring the distance between SCD peaks. Here the rate is found to be approximately 143 Hz.

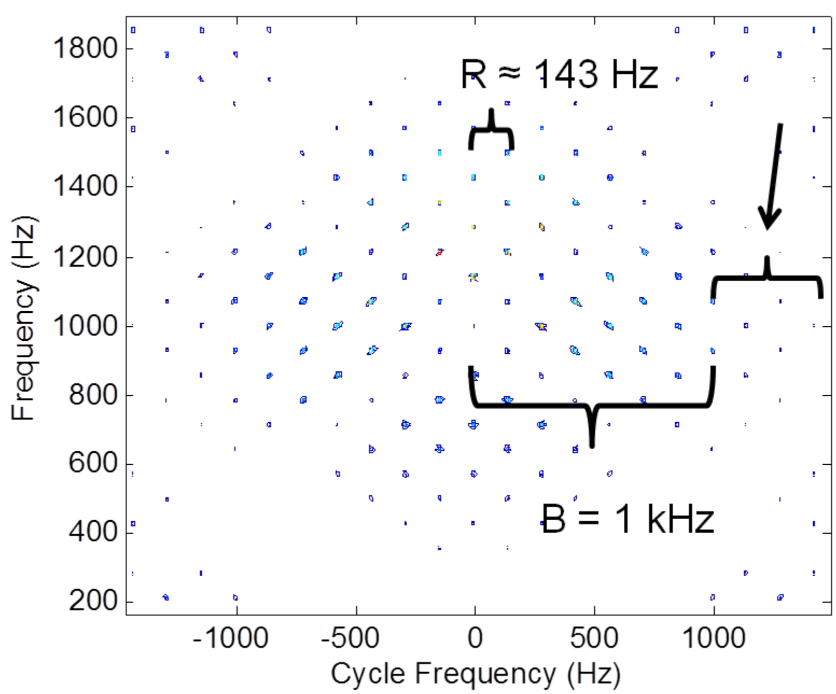

Figure 2.12: Annotated and zoomed view of a 7 bit barker code BPSK signal DFSM SCD

2.6 Communication with Noise Radar

Some type of encoding is needed to perform any type of communication. For example, when two people talk, the language they speak is a type of encoding. If both individuals know the language that is being spoken, they can communicate effectively. When communication is performed using RF the concept is no different; both the transmitter and receiver need to know the language or encoding technique that is being employed. For the purposes of this research, a basic encoding technique will be employed by using 128 unique templates. Each template will be assigned to an American Standard Code for Information Interchange (ASCII) character. This basic encoding technique is employed to demonstrate the ability to perform communication using the noise waveform. By using this encoding technique, the rate at which characters are transmitted will be the length of the templates. For example, if the each template is 1 μs long, the maximum character transmission rate will be 1 MHz. The receiver for the communication system will utilize the matched filter. This is the same process that is outlined in Section 2.2.

2.7 Chapter Conclusion

General radar theory as it pertains to a RNR system was discussed. The concept of LPI was introduced, and three different techniques of detecting and classifying LPI radars were introduced. These techniques will be utilized to compare LPI properties of an analog generated RNR waveform to the properties of a digitally generated RNR waveform. Finally, the concept of performing communication using the RNR waveform was presented and a specific encoding technique was established. Chapter 3 will focus on describing the AFIT RNR and will cover the modifications performed to allow simultaneous communication and radar using a digitally generated noise waveform.

III. System Description and Methodology

3.1 Chapter Overview

To determine if a fully digital noise radar has nearly the same performance as the current Air Force Institute of Technology (AFIT) random noise radar (RNR), a methodology and test plan were established. An overview of the current system hardware and software is presented in this chapter. A plan to modify the components and the methodology for testing the modified components is presented. Additionally, the techniques needed to make a thorough analysis is explained.

3.2 System Description

The AFIT RNR was developed by Schmitt and was used for through the wall sensing in a bistatic configuration [22]. The software was modified by Nelms and Thorson to improve the digital signal processing speed [17, 23]. Figure 3.1 shows a functional diagram of the AFIT RNR. The noise source in Figure 3.1 contains the noise generator, a low pass filter, a high pass filter, and a splitter. The receiver hardware includes two low noise amplifiers (LNAs), a low pass filter, and a high pass filter.

3.2.1 RNR Transmitter.

The AFIT RNR transmitter is comprised of the antenna, the noise generator, a low pass filter, a high pass filter, and a splitter (power divider). Figure 3.2 highlights the internal transmitter components. The noise source uses a noise diode to generate thermal noise. This thermal noise source generates white Gaussian noise from 100 Hz to 1.5 GHz. This thermal noise source is manufactured by Noise Comm Inc. The low pass filter is manufactured by Mini-Circuits and passes frequencies DC to 720 MHz. The high pass filter is manufactured by Mini-Circuits and passes frequencies 395 MHz to 3.2 GHz. The low and high pass filters create a bandpass filter from 395 MHz to 720 MHz, which

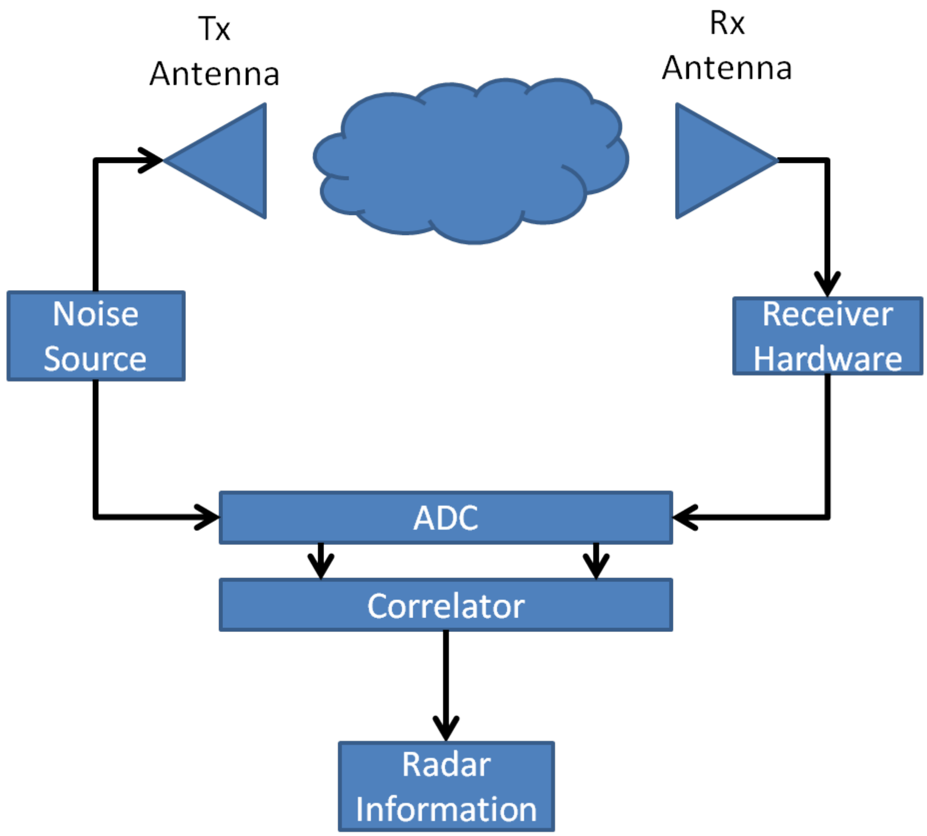

Figure 3.1: Functional diagram of AFIT's RNR

matches the antenna bandpass frequencies and reduces the reflections to the AFIT RNR. The splitter is from Mini-Circuits and has a frequency range of 10 to 1500 MHz. One splitter output is connected to the antenna, and the other is connected to the analog to digital converter (ADC); thus, the RNR samples the noise signal that is sent to the transmit antenna. Table 3.1 shows the specifications of each of the transmitter components.

3.2.2 RNR Receiver.

The AFIT RNR receiver is comprised of the antenna, two low noise amplifiers (LNAs), a low pass filter, and a high pass filter. Figure 3.3 highlights the internal receiver components. The antennas for both the transmitter and receiver, which are printed circuit board (PCB) log periodic antennas (LPAs) that operate from 400 to 1000 MHz. The low

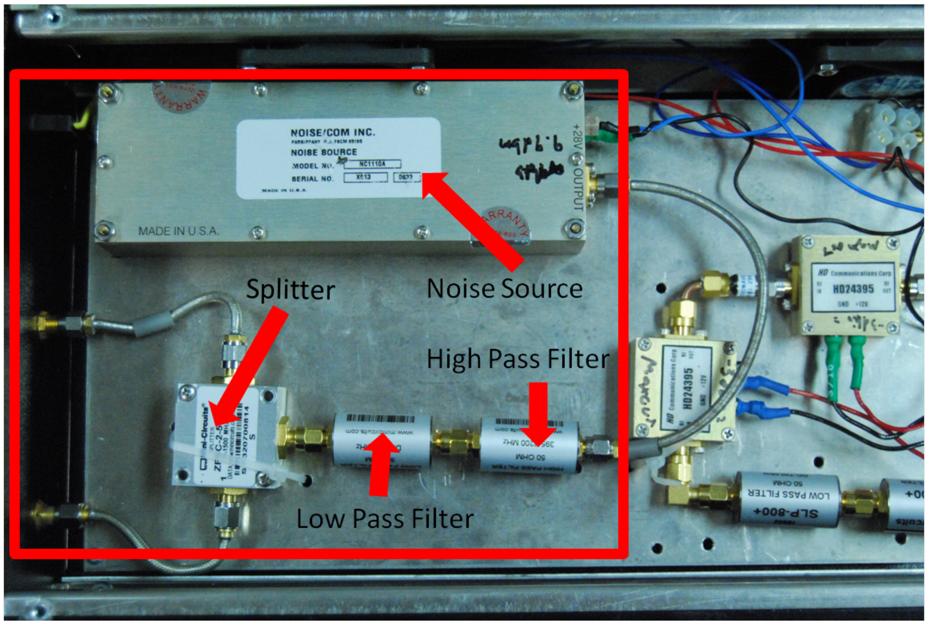

Figure 3.2: Internal AFIT RNR transmitter components

Table 3.1: Transmitter Components

Component	Manufacturer	Model	Frequency Range
Noise Source	Noise Comm Inc	N1110A	100 Hz - 1.5GHz
Splitter	Mini-Circuits	ZFSC-2-5	10 MHz - 1.5 GHz
Low Pass Filter	Mini-Circuits	SLP-800+	DC - 720 MHz
High Pass Filter	Mini-Circuits	SHP-400+	395 MHz - 3.2GHz

pass and high pass filters are the exact same specifications and manufacture as the filters in the transmitter side. The LNAs are manufactured by HD Communications Corp. and have a 19 dBm gain from 100 MHz to 1.4 GHz. Two LNAs in the AFIT RNR give the received signal a 38dBm boost in power. The received signal first enters the filters to reduce the amount of noise generated by the amplifier and to increase the signal-to-noise ratio (SNR). Table 3.2 shows the specification of each of the receiver components.

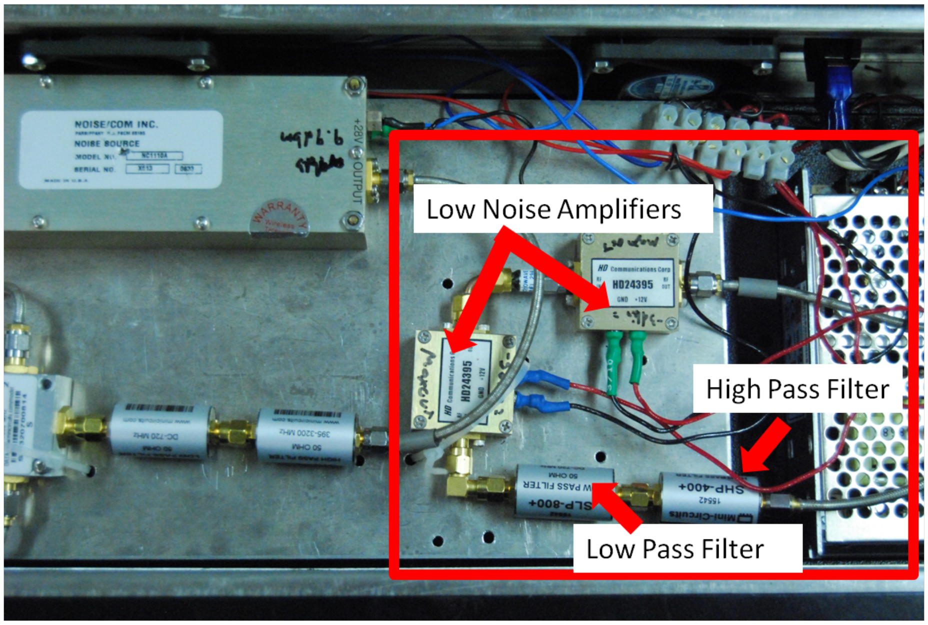

Figure 3.3: Internal AFIT RNR receiver components

Table 3.2: Receiver Components

Component	Manufacturer	Model	Frequency Range
Low Noise Amplifier	HD Comm	HD24395	100MHz -1400MHz
Low Pass Filter	Mini-Circuits	SLP-800+	DC - 720 MHz
High Pass Filter	Mini-Circuits	SHP-400+	395 MHz - 3.2GHz

3.2.3 Software.

The current NoNET software has been refined through the efforts of several previous students and now includes main programs for performing near monostatic and netted monostatic radar [17, 19, 23]. The netted monostatic radar is a mode where each radar unit acts independently, but shares the transmit and receive waveforms with a central node. Also included in the software suite is a routine to calibrate the AFIT RNR. The NoNET software has many additional functions to support the main radar functions. Figure A.1 shows the major functions and how the near monostatic software algorithm performs.

To perform the netted monostatic radar, the AFIT NoNET uses the monostatic radar at each of the radar nodes but then shares the transmitted and received waveforms over a local area network (LAN) network. An example of how the the netted monostatic radar is configured is shown in Figure 3.4. Here there are two nodes, a central node, and a target.

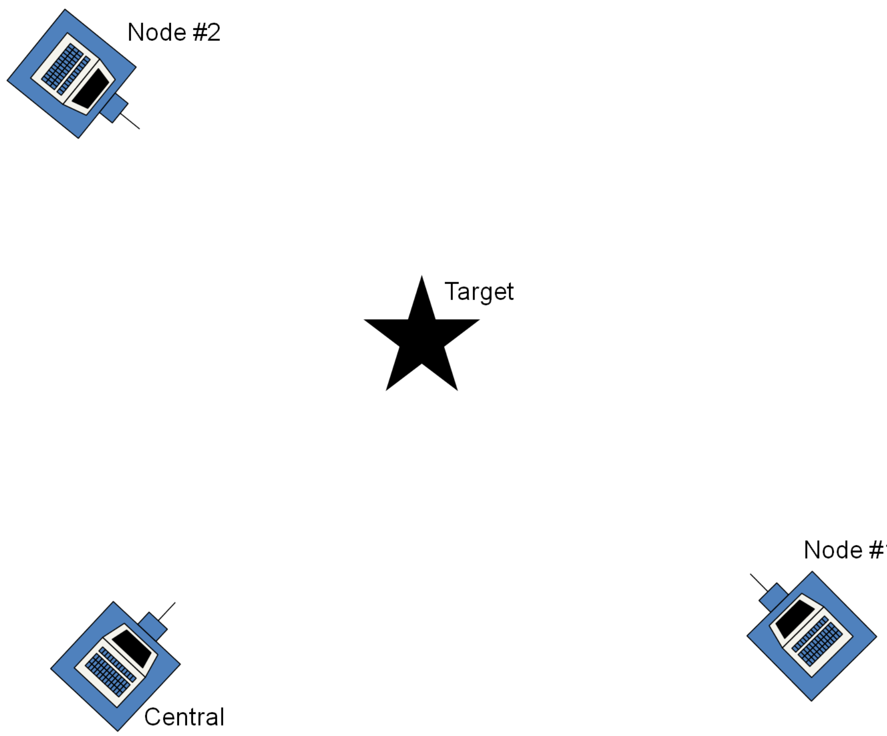

Figure 3.4: Example of AFIT RNR setup in netted monostatic configuration

Each RNR node will range the target and share its transmit and receive waveforms with the central node where the central node does the netted monostatic radar signal processing. The netted monostatic NoNET algorithm flow diagram is shown in Figure A.2. The other support programs allow for the setup of the capture cards, signal processing, and plotting the final results.

3.3 Modifications

This section will describe the modifications made to the transmitter, the receiver, and the software to include the digital waveform generator. Since modifications were planned a total redesign of the system was contemplated. The intent was to keep as much of the original system as possible, but the objective was to make the system extremely flexible and have complete software control of the components. Another objective was to put all of the components into a single unit. Putting all the components into a single unit allows for a more mobile compact platform. The plan is diagrammed in Figure 3.5.

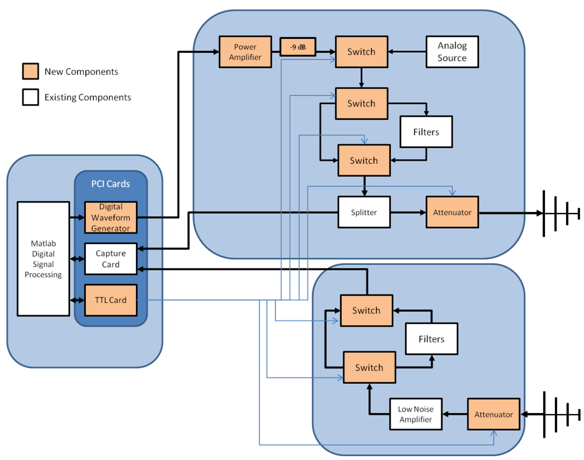

Figure 3.5: Planned modifications to existing system to incorporate system requirement objectives

To better achieve the objective of housing all the components into a single box, the Magma 4 slot PCI Expansion box seen in Figure 3.6 was selected to house the AFIT RNR. To use this box for the AFIT RNR, it needed to be modified to allow for the transmission and receiving componets to fit inside. The bay where hard-drives were made to sit was modified to allow for an aluminum tray seen in Figure 3.7 to be placed which will hold the radar components. Underneath the aluminum tray is the analog noise source and a $+24V$ DC power supply to power the noise source. The power supplied to the radio

Figure 3.6: Magma 4 Slot Peripheral Component Interconnect (PCI) Expansion Box

frequency (RF) components on top is provided by the $+3V$ and $+12V$ from the ATX power supply included in the Magma box.

Figure 3.7: Modified Magma PCI Expansion Box with AFIT RNR components

The major contributor forcing the modification of the current system is the addition of the digital waveform generator. This addition will enhance the AFIT RNR capabilities by facilitating further research on using the noise waveform for simultaneous communication and radar. The digital waveform generator is manufactured by Chase Scientific Company.

It is a 4 GS/S PCI arbitrary waveform generator with the ability to store 16 Mega Words or 32 Mb of waveform information.

To control all the switches and the digital step attenuators, a transistor-transistor logic (TTL) PCI card was needed. The card that was chosen was Advantech's PCI-1739U, which is a 48 channel TTL and can be configured as either digital input or output. The current modifications only require use of 24 channels; therefore 24 channels are left for future configuration.

The transmission side of the AFIT RNR was modified with the planned changes shown in Figure 3.5. This included three RF switches, a power amplifier, and a digital step attenuator. The RF switches are TTL controlled and are manufactured by Mini-Circuits. They have a frequency operating range from DC to $3GHz$. Table 3.3 shows the three positions that the switches can be configured.

Table 3.3: Truth Table for RF Switch

Control Input		RF Input/Output	
Control 1	Control 2	RF1 to Common	RF2 to Common
Low	Low	OFF	OFF
Low	High	OFF	ON
High	Low	ON	OFF
High	High	N/A	N/A

The first switch after the noise source selects between the digital waveform generator and the analog noise source. The next two switches work together to switch between using the hardware filters and bypassing the filters. This was implemented to allow for the full bandwidth of the analog noise source or for use with the digital waveform generator and software filtering. A main consideration in using these switches are their design, shown in

Figure 3.8, that incorporates a 50 Ω load on each of the legs for when the switch deselects the corresponding port.

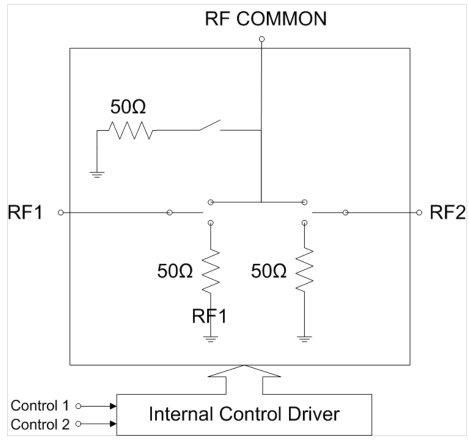

Figure 3.8: Switch functional diagram [13]

The power amplifier is placed on the digital waveform generator to increase the signal out of the waveform generator. By amplifying the digital signal the frequency spectrum amplitude more closely matches the signal strength from the digital waveform generator to the power out of the analog signal. A 9 dB fixed inline attenuator was placed after the amplifier because the gain of the amplifier was much more than what was required to bring the digital waveform generator power level up to the level of the analog noise source. The amplifier is manufactured by HD Comm with a bandwidth of 100 MHz - 1000 MHz. The specific parameters of the amplifier are detailed in Table 3.4.

Table 3.4: Amplifier Parameters

Parameters	Value
Frequency Range	100 - 1000 MHz
Gain	45dB
Noise Figure	3.5dB

The digital step attenuator is manufactured by Mini-Circuits and has a max 31.5 dB attenuation that is software controllable in 0.5 dB steps. This software control is done with a TTL level signal. The addition of the digital step attenuation to the system allows the operator to dial in attenuation to reduce the amount of self-induced noise. This is especially useful when operating in a multistatic situation where there are multiple noise radars transmitting nearby. Additionally, more attenuation might be needed to reduce the amplitude of the reflection when trying to use the radar in a through the wall sensing scenario.

There were not as many changes made to the receiver as there were to the transmitter side. The only changes were the ability to bypass the filters and the adding the attenuator. The switches and the attenuator are the same models as the ones on the transmitter side.

3.4 Test Methodology

The test methodology follows the crawl, walk, run approach. First the system was characterized, and the analog source compared to the previous system to ensure that current and previous systems are similar. This enables analysis obtained within this research to be compared to the previously accomplished research [19] [17]. The main factors that will be considered are the spectrum and the statistical distribution of the captured signal. The next step is to compare the analog signal to the digital signal.

The comparisons between the analog and digital waveforms was limited to the analysis techniques for detecting low probability of intercept (LPI) parameters. These techniques were chosen to analyze the current system, because comparisons can be directly made with the previous research [19]. The test methodology for these tests will be described in Section 3.4.2. Finally, after the comparison between the analog and digital waveforms was accomplished, the analysis of using the RNR waveform for communication was performed. This test setup is described in Section 3.4.3.

3.4.1 System Verification.

The purpose of performing the system verification is to ensure the current system is similar to the previous system. First, the spectrum of the transmitter will be compared. The previous system configuration transmitter output is connected to the spectrum analyzer in the Radar Instrumentation Laboratory (RAIL). The spectrum analyzer is step up to measure 50 MHz to 2.5 GHz in 3 MHz steps. Then the modified system is connected to the spectrum analyzer with the same settings. The spectrum analyzer is set so the output amplitude is not normalized. However, the output amplitude is a relative measurement, meaning that a comparison can be made between two measurements but the absolute measurement may not be accurate.

Similarly, the frequency spectrum between the analog and digital sources is compared. The spectrum analyzer is setup with the same settings as the previous system and current system comparison. The spectrum analyzer is connected to the AFIT RNR transmitter output. Table 3.5 shows the measurements that are taken to compare the digital to the analog sources.

Table 3.5: Frequency spectrum measurements comparing analog and digital sources

Source	Filters
Analog	ON
Analog	OFF
Digital	ON
Digital	OFF

The next system verification experiment is to verify the current system performance in performing radar. For this experiment the AFIT RNR is setup and a calibration is performed. The calibration in the AFIT RNR consists of placing a target at a known

distance between 3 - 5 meters. Then a ranging operation is performed, and the result is calculated and given as the estimated range. This estimated range is then compared to the actual range that is entered by the user. The difference between the estimated range and the entered range is the error and this error is stored in the calibration for future use in the radar operation. After calibration the AFIT RNR is placed into the background subtraction mode, where the first capture of the radar is the background environment. The user is then prompted to place the target into the scene. After the target is placed into the scene the radar performs a background subtraction for the length of the requested radar operation.

Using the analog source with the filters turned on the AFIT RNR a calibration is performed with the calibration target setup at 3.12 m. After calibration the target is setup at 4.9 m. Then the system is switched to use the digital source with the filters turned on. The calibration is re-performed with the calibration target at 4.12 m. The target is then placed at 4.7 m and the ranging operation is performed. The expected uncertainty in the AFIT RNR ranging operation is given as 6.79 cm [17].

3.4.2 LPI.

The purpose of this experiment is to determine the detectability of the digitally generated waveforms. To accomplish this experiment, a single AFIT RNR node that has been modified according to Section 3.3 is used to transmit both the analog and digital waveforms. The receiver location is determined by comparing the background signal amplitude displayed on the oscilloscope to the transmitted analog noise signal. When these signals are at approximately the same amplitude, the receiver location is set and not moved. The actual signal-to-noise plus interference ratio (SNIR) will be calculated during the post processing. By determining the SNIR when the transmitter attenuation is set at 0 dB, negative SNIR values can be determined by increasing the attenuation in the transmitter. Figure 3.9 shows the setup of this experiment. This experiment was performed in the hallway outside of the AFIT Advanced Navigation Technology (ANT) Center aviary. The

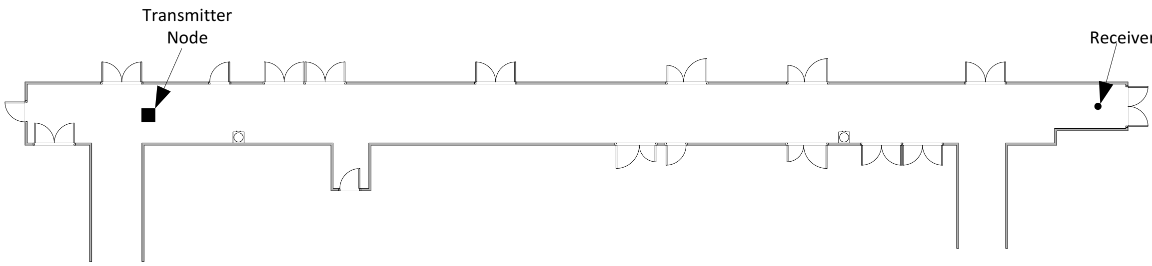

Figure 3.9: Diagram of LPI experimental setup

receiver will be comprised of a EMCO double ridged guide antenna and an oscilloscope that has the capability of sampling the received signal greater than 3 GHz. This EMCO horn

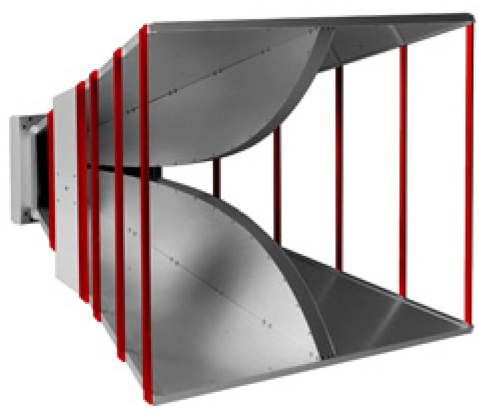

Figure 3.10: EMCO horn antenna used to collect LPI analysis data

has a fairly constant gain over the frequency range of 395 MHz - 720 MHz. Figure 3.11 shows the gain curve from the EMCO 3106B datasheet. This antenna was chosen due its high gain, thus representing an antenna that might be used in an attempt to intercept a noise radar signal. The oscilloscope with a large sampling rate was selected to increase the bandwidth in the captured signal. The oscilloscope to be used is a Tektronics Model# DPO 7354, available in the RAIL.

The measurements in Table 3.6 will be taken for this experiment. Each measurement in Table 3.6 is a single capture at 5 GHz lasting 200 μs between each capture the transmitter attenuation is increased. Each of these measurements will be post processed using the

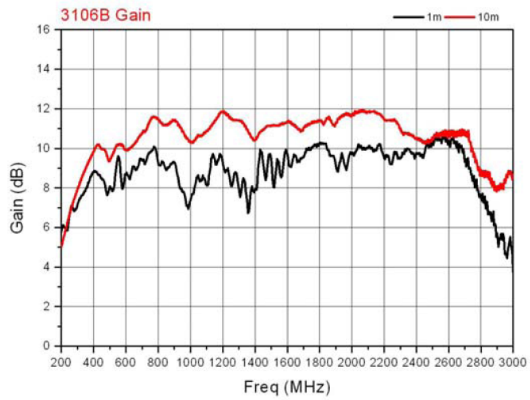

Figure 3.11: EMCO 3106B antenna gain pattern [3]

Autocorrelation, quadrature mirror filter bank (QMFB), and Cylcostationary processes to determine if there are any parameters can be determined.

Table 3.6: LPI Measurements

Source	Tx Attenuation
None	0
Analog	0
Analog	3
Analog	6
Analog	24
Digital	0
Digital	3
Digital	6
Digital	24

3.4.3 Communication.

The purpose of this experiment was to show that the RNR waveform can be used as a waveform for digital communication. The receiver node is initially placed at 10 ft, and a series of 10 captures lasting 1 ms are taken. The receiver is then moved another 10 ft, and the process is repeated until the final distance of 150 ft is recorded. This setup is shown in Figure 3.12. The received symbol error rate (SER) from the data collected at each distance provides a measure of how well the systems can communicate over a given distance.

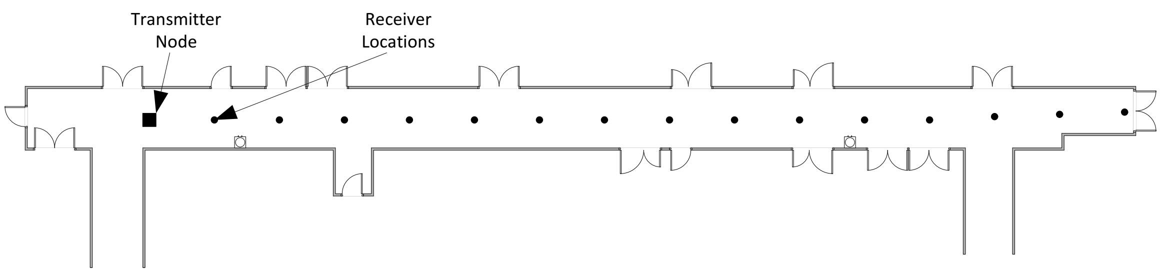

Figure 3.12: Diagram of communication experiment setup

The phrase “Hello World. This is a test message” is transmitted using a simple one-to-one encoding of American Standard Code for Information Interchange (ASCII) characters-to-templates. Table 3.7 shows the distribution of letter within the phrase.

To decode the received message and determine a SER, where symbols are the digitally generated noise templates where each template represents anASCII character. The received message was broken into “bins” of length equaling the transmitted template length, these bins were each then be correlated against every template. The template with the maximum correlation is the estimated as the transmitted template. To determine the SER, the estimated received template is compared to the actual transmitted template, and any difference counted as an error.

Table 3.7: Distribution of ASCII characters in the transmitted message: "Hello World. This is a test message"

ASCII Decimal	Character	Count
32	space	32
46	.	1
72	H	1
84	T	1
87	W	1
97	a	2
100	d	1
101	e	4
103	g	1
104	h	1
105	i	2
108	l	3
109	m	1
111	o	2
114	r	1
115	s	5
116	t	2

3.5 Chapter Conclusion

The current AFIT RNR system was described, and the modifications that enabled the addition of the digital waveform generator were explained. The test methodology for determining the LPI classification was laid out. The methodology for demonstrating communication encoding on a noise waveform was detailed. Finally, the process for

determining the SER was explained. The information contained in this chapter will serve as the basis for the experimental results analyzed in Chapter 4.

IV. Results and Analysis

4.1 Chapter Overview

This chapter provides the analysis of the data collection explained in Chapter 3. This analysis will first compare the previous Air Force Institute of Technology (AFIT) random noise radar (RNR) to the current system after the modifications explained in Chapter 3 have been performed. Next the analog and digital source outputs will be compared. This will provide a basis for the rest of the analysis and a foundation to make comparisons in the detectability of the RNR waveforms. Autocorrelation, quadrature mirror filter bank (QMFB), and cyclostationary analysis were performed on both the analog and digital waveforms to determine if parameters are able to be extracted. Finally, using a simple one-to-one encoding scheme, the effect of encoding information on the RNR will be analyzed and a simulated symbol error rate (SER) will be compared to the experimental SER.

4.2 Modification Verification

To verify the modifications discussed in Chapter 3 did not change the output transmission signal significantly, the spectrum from the unmodified system and the modified system are compared. Figure 4.1 shows the comparison of the transmitted waveform in the previous system and the modified system. The previous system has an average power of -26.13 dBm over the frequency range 307 MHz - 803 MHz. Where the current system has an average power of -30.81 dBm over the frequency range 307 MHz - 803 MHz, resulting in a 4.68 dBm difference. Insertion losses for the additional components in the transmission side are shown in Figure 4.2.

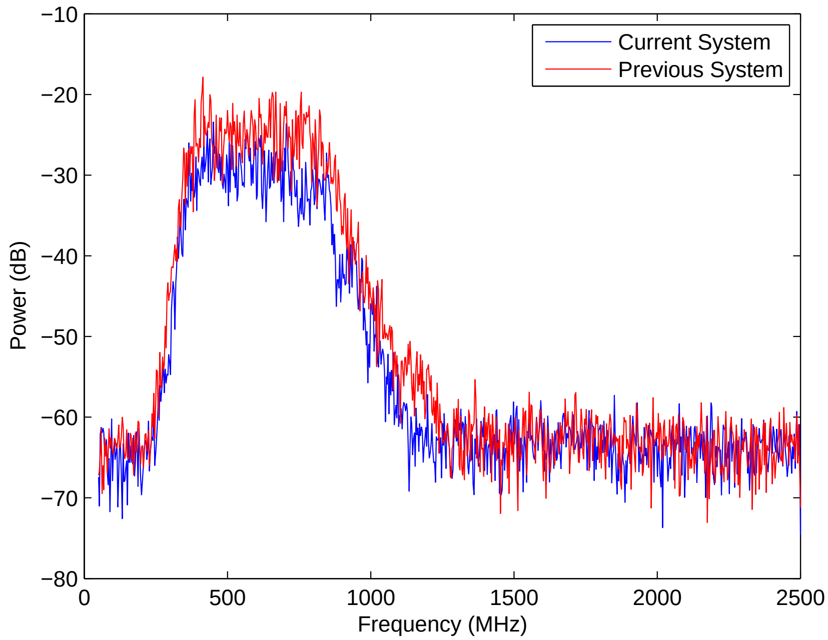

Figure 4.1: Comparison between previous system and the current system after modifications, with the filters turned on

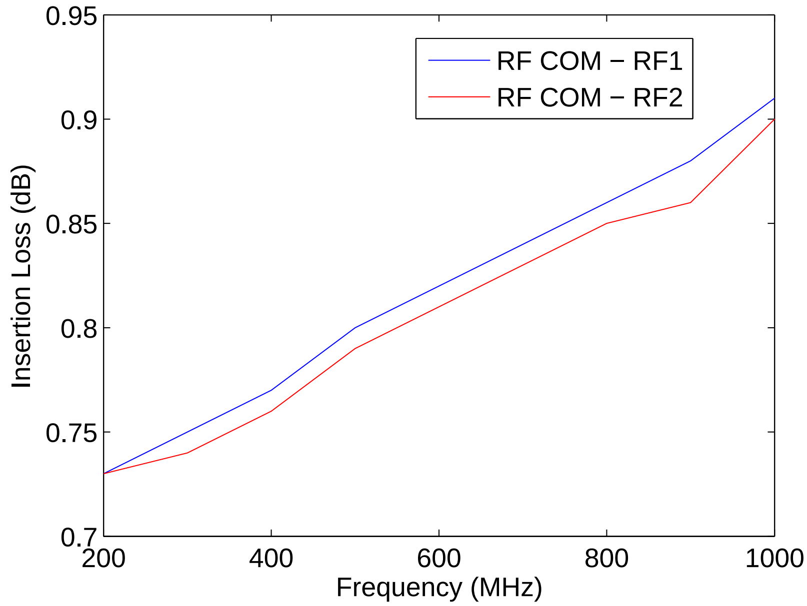

(a) Insertion loss for radio frequency (RF) switches [14]

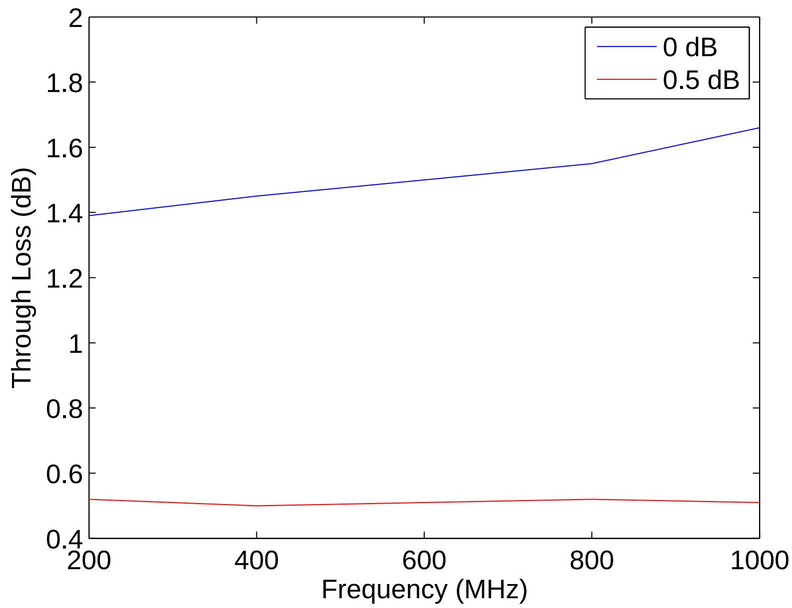

(b) Insertion loss for attenuator at 0 dB [12]

Figure 4.2: Insertion loss for additional components in the modified AFIT RNR

Using the average insertion losses over the frequency range, the three switches, and one attenuator, the total insertion loss comes to 4.03 dB over the frequency range 400 MHz - 800 MHz. This accounts for the losses seen in Figure 4.1. The biggest contributor to the total insertion loss is from the attenuator. The attenuator manufacturer provides typical loss values for each attenuation level; Figure 4.2(b) is the 0 dB attenuation level. Since the average typical loss is greater than the lowest non-zero attenuation step, as seen in Figure 4.2(b), the attenuator should be set to use the 0.5 dB attenuation level in an attempt to minimize the attenuator contribution.

4.3 Analog vs Digital

Other than the small losses through the switches and the attenuators, the previous system and the current system have nearly the same output characteristics. Now when making a comparison between the digital source and the analog source there is traceability to previous research. The first comparison is the unfiltered spectrum shown in Figure 4.3.

The slope of the digital signal output is due to the digital waveform generator itself. The decreasing power is seen on the direct output Figure 4.4; however, it is not as severe as in Figure 4.3. The additional attenuation that is shown in the higher frequencies can be attributed to the higher attenuation through the switches and the attenuator as shown in Figure 4.2.

When the filters are turned on, the power for the digital waveform generator between 300 MHz and 800 MHz is fairly flat, as seen in Figure 4.5. The average power difference between the analog and digital sources for frequencies of 300 MHz to 800 MHz is 5.95 dB. The relative power level for the digital source for the frequency range 300 MHz to 800 MHz is -26.59 dB. Recall from Section 4.2 the previous system's average power level is -26.13 dB. Therefore, the power that has been lost thorough the switches and the attenuator is reclaimed when using the digital source.

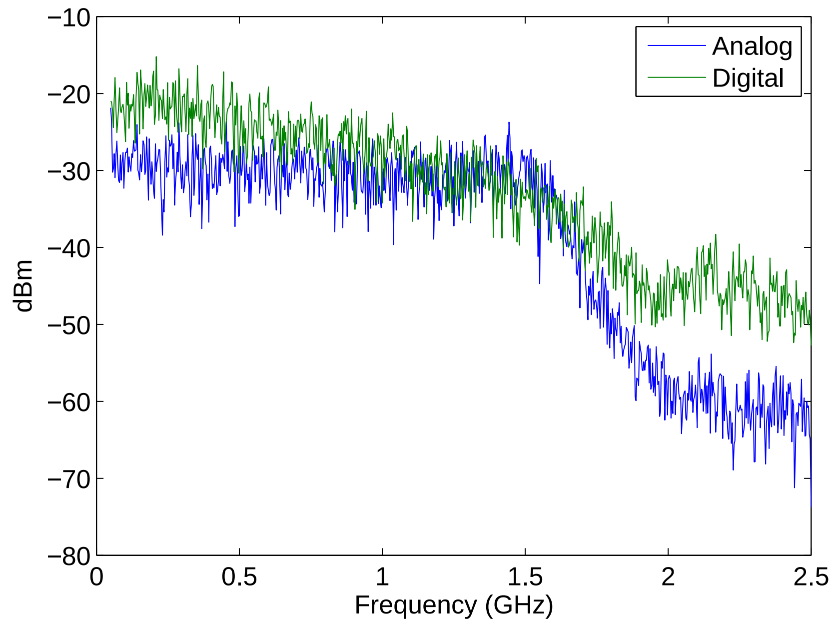

Figure 4.3: Unfiltered spectrum comparison between the analog noise source and the digitally generated noise source

The distribution of transmitted waveform voltages are shown in Figure 4.6. Using Equation 2.25 to estimate the transmitted power, the average transmitted power for the analog source is -20.23 dB and for the digital source is -14.58 dB, yielding a difference of 5.65 dB. In Figure 4.5 there is a difference of 5.95 dB between the average power in the frequency range 300 MHz to 800 MHz. Since the power averages are approximately equal the differences in transmission statistics, in Figure 4.6 are due to the power differences.

To ensure that the RNR functions the same with both the analog source and the digital source, a simple ranging experiment was performed. The results are displayed in Figure 4.7. For the analog source, the target was setup at a range of 4.9 m, and for the digital source the target was at 4.7 m. For both the analog and digital sources, a calibration was completed and the radar was placed in the background subtraction mode. The radar performed very well and was able to accurately range the given target. This provides a very good check that the system is operating properly in both operation modes. Additionally,

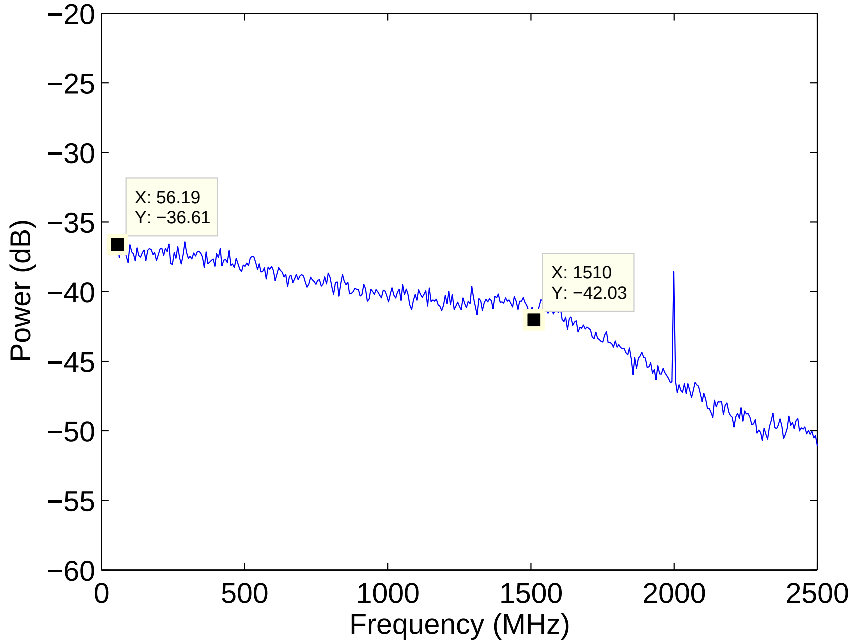

Figure 4.4: Direct output power from digital waveform generator.

this provides the confirmation that there is little difference between the digital and analog sources when used to perform radar.

4.4 Detectability

Since the digital source and the analog source are similar, comparisons in the detectability are able to be made. This is important because a truly white Gaussian noise (WGN) waveform is very difficult to detect and determine specific radar parameters. This section will cover three types of detectability analysis; autocorrelation, QMFB, and cyclostationary analysis. The QMFB and the cyclostationary analysis are performed using a qualitative visual assessment. This assessment provides the user the ability to recognize patterns and features that are present in the results. Currently there is no adequate way to perform this analysis using a quantitative assessment. The process outlined in Chapter 3 was followed, and the distance at which the received signal was approximately 0 dB signal-to-noise plus interference ratio (SNIR) was at 42.25 meters. At 42.25 meters, the SNIR is

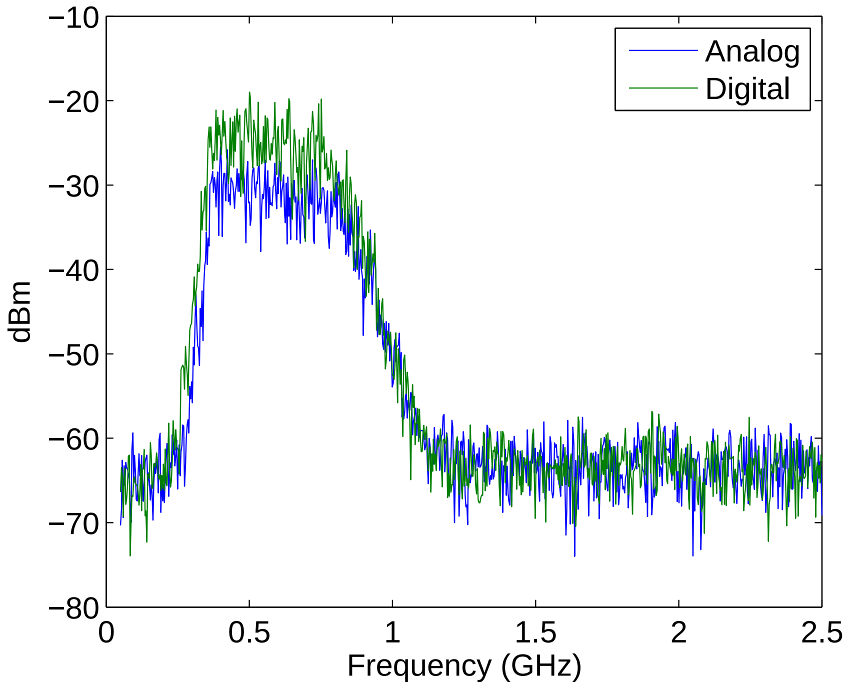

Figure 4.5: Filtered spectrum comparison between analog and digital outputs

calculated by using the estimated power explained in Section 2.4. The when the transmitter attenuation is set to 0 dB, the analog SNIR is calculated at 2.36 dB, and the digital source SNIR is calculated as 5.97 dB. Therefore, by adjusting the calculated SNIRs with the additional transmission attenuations, negative SNIR values calculated and are shown in Table 4.1.

4.4.1 Autocorrelation Analysis.

When analyzing a random waveform's autocorrelation it is important to remember what the autocorrelation provides. As discussed in Chapter 3, the autocorrelation provides a means to determine if a signal has repetition within itself. Correlation of two uncorrelated random signals are shown in Figure 4.8, illustrating what would be seen if there is no correlation between random signals. Figure 4.9 shows the transmitted signal from an analog source at various SNIR levels. These SNIR levels are approximate and are derived

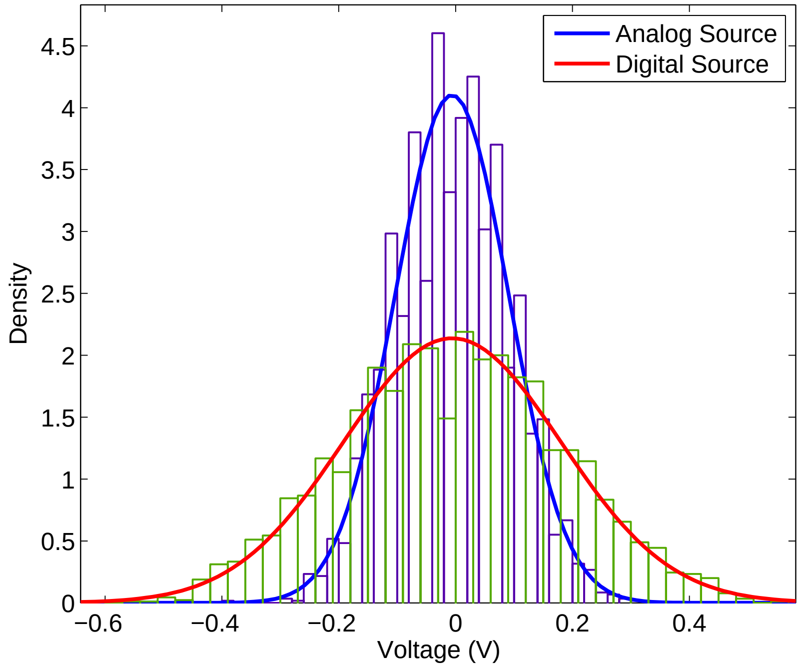

Figure 4.6: Analog and digital transmission statistics

Table 4.1: low probability of intercept (LPI) measurement SNIR levels

Source	Tx Attenuation Setting	Calculated SNIR
Analog	0 dB	2.36
Analog	3 dB	-0.64 dB
Analog	6 dB	-3.64 dB
Analog	24 dB	-21.64 dB
Digital	0 dB	5.97 dB
Digital	3 dB	2.97 dB
Digital	6 dB	-0.03 dB
Digital	24 dB	-18.03 dB

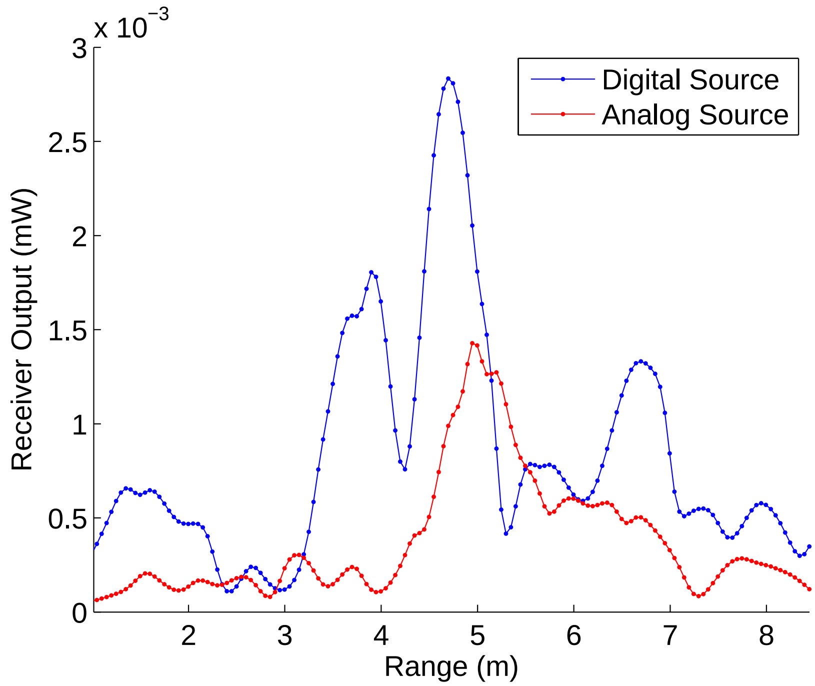

Figure 4.7: Analog and digital radar function check, using the radar ranging function to make the comparison

based on the setup of this experiment as described in Chapter 3. Within the transmitted waveform from the analog source there is no correlation peaks other than at 0 lag. This says that there is no repetition with in the analog source signal. This is anticipated, due to the design of the analog noise source. The purpose of this analysis is to serve as the baseline for the digital analysis.

The autocorrelation for the transmitted waveform from the digital source are shown in Figure 4.10. At SNIR equal to 5.97 dB, 2.97 dB, and -0.03 dB the repetition is noticeable. By measuring the time between each peak, the repetition period of the entire sequence is determined to be 35.84 μs. When the SNIR is greater than 0 dB some subsections of the templates are noticible. In the case where the SNIR is equal to 5.97 dB, the time between some of smaller peaks are measured to be 1.024 μs. At other smaller peaks the time difference is measured to be 3.072 μs, 2.05 μs, and 16.38 μs as seen in Figure 4.11.

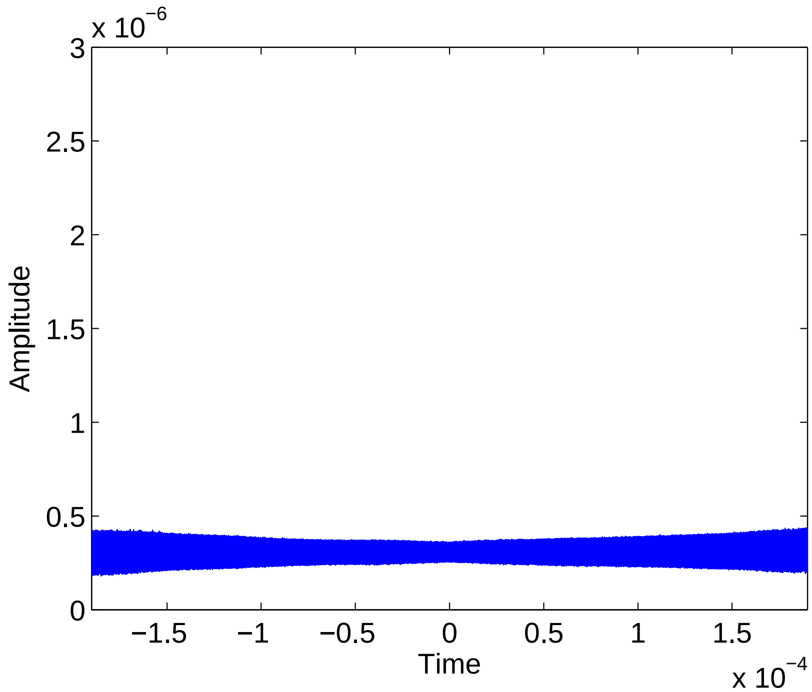

Figure 4.8: Cross correlation between two random signals, illustrating no correlation peaks for two uncorrelated random signals

An observer with no knowledge of the actual transmission might guess that the smallest time difference of 1.024 μs is the length of a single transmission template. This guess would be correct and possibly would allow the observer to use this information to decode the received waveform. Once the SNIR is below 0 dB there is no noticeable repetition of the individual templates.

In Figure 4.10(d), the individual characters are not picked up in the transmission. This is attributed to the length of each template that represents a character being short enough and the SNIR being small enough that the correlation peaks do not rise above the noise of the correlation. The significance of this result is that the amount of repetition within a message is not as significant as the entire message being repeated. This will allow for the simplest encoding technique to be used and will not require a more complicated encoding scheme. Limiting the number of times a message is transmitted will help preserve the LPI

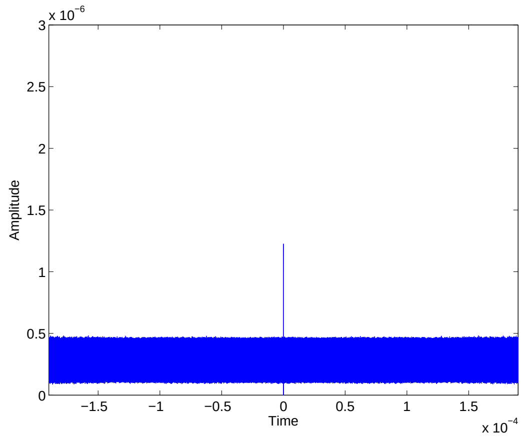

(a) SNIR = 2.36 dB

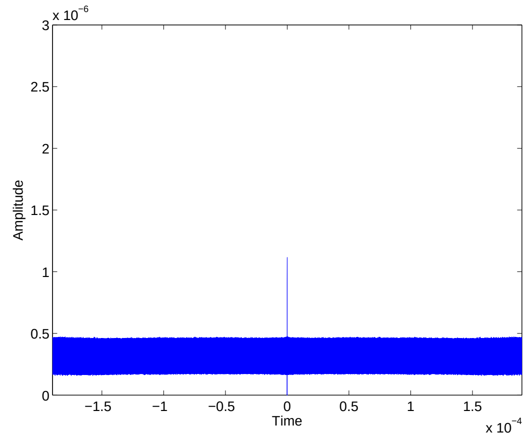

(b) SNIR = -0.64 dB

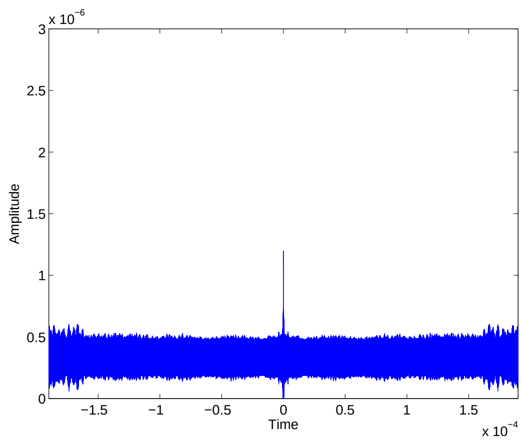

(c) SNIR = -3.64 dB

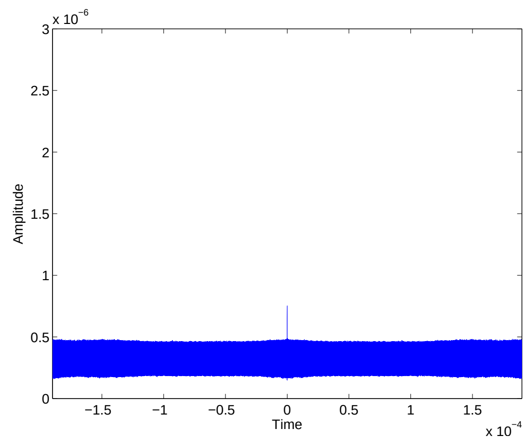

(d) SNIR = -21.64 dB

Figure 4.9: Analog source transmitted waveform autocorrelation at different SNIR

characteristics. In Figure 4.10(c) the autocorrelation noise looks very sinusoidal; this is an unknown phenomenon and is only seen very rarely. It is thought to be from an external interfering signal within the same frequency band.

4.4.2 QMFB Analysis.

As shown in Section 4.4.1, the best chance of detecting the digital transmission lies in the SNIR of 0 dB. Figure 4.12 shows the third layer contour plot for the approximated 0 dB SNIR signal. Using the binary phase shift keying (BPSK) plots in Section 2.5.2 as a

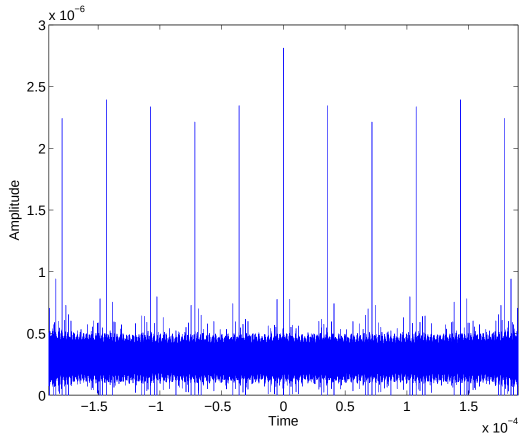

(a) SNIR = 5.97 dB

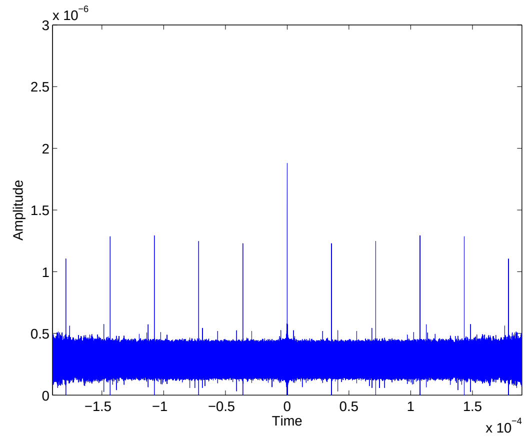

(b) SNIR = 2.97 dB

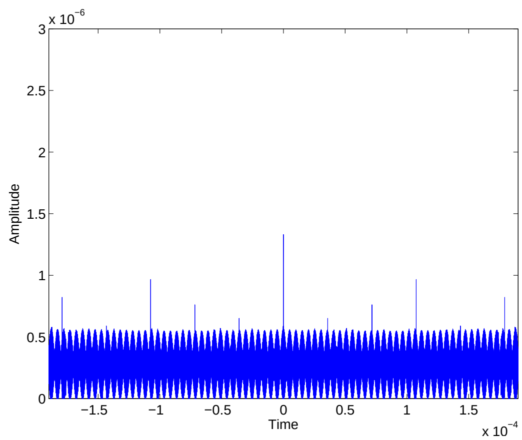

(c) SNIR = -0.03 dB

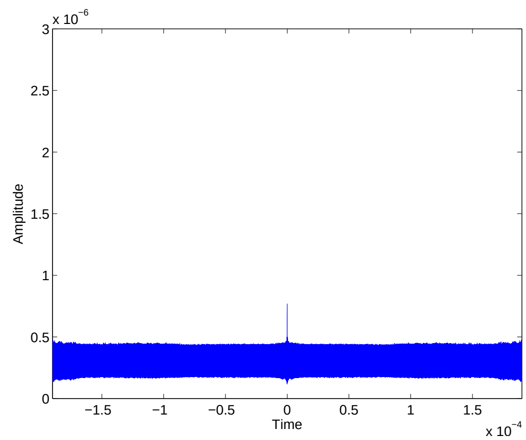

(d) SNIR = -18.03 dB

Figure 4.10: Digital source transmitted waveform autocorrelation at approximately various SNIR

reference, there is no information gained by using the QMFB for determining pulse period. Even with the a priori knowledge that the individual template length is 1 μs, template length is unable to be determined as shown in Figures 4.13.

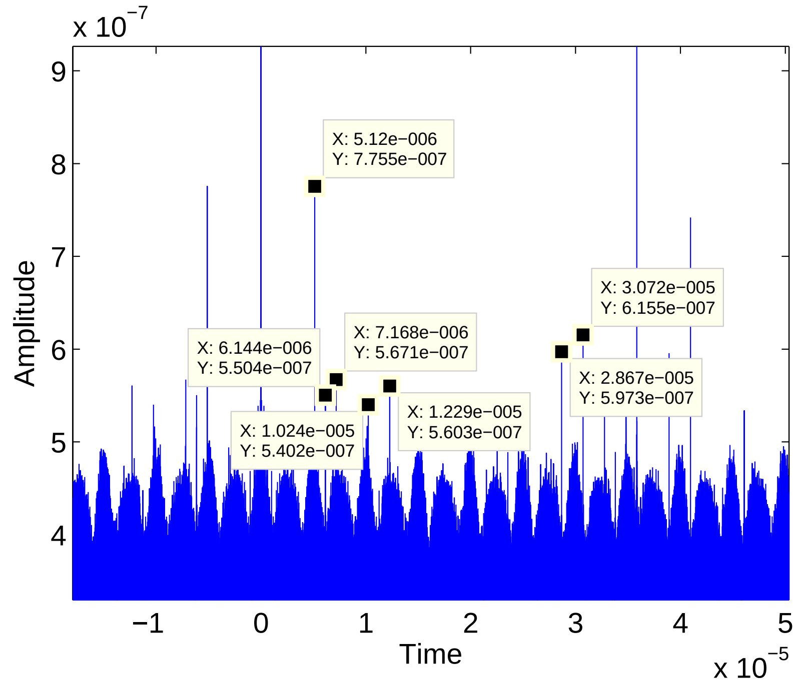

Figure 4.11: Digital source transmitted waveform autocorrelation at SNIR = 5.97 dB, illustrating the small correlation peaks

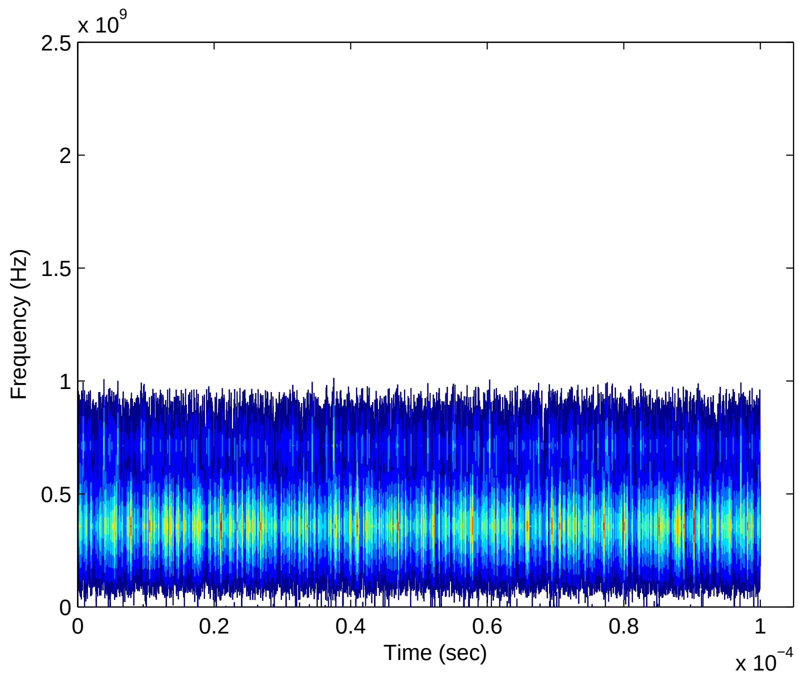

Figure 4.12: QMFB layer 3 contour plot of received signal from digital transmission at approximately 0 dB SNIR

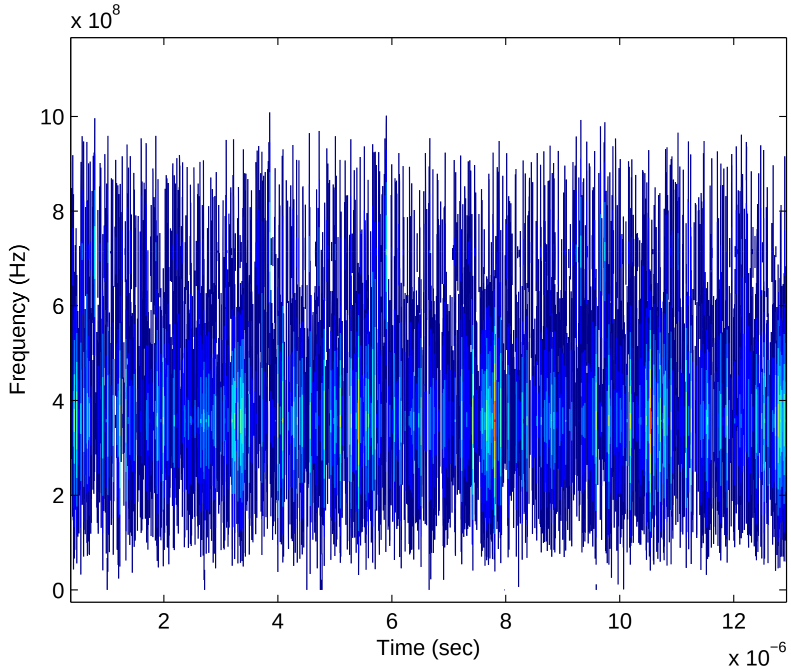

Figure 4.13: QMFB layer 3 contour plot of received signal from digital transmission at approximate 0 dB SNIR, zoomed in view to look for individual template length

The other parameter that can be determined using the QMFB analysis is bandwidth of the transmitted signal. Figure 4.14 shows the color plot of four differing SNIR levels for the analog source transmission. The background capture was subtracted from each

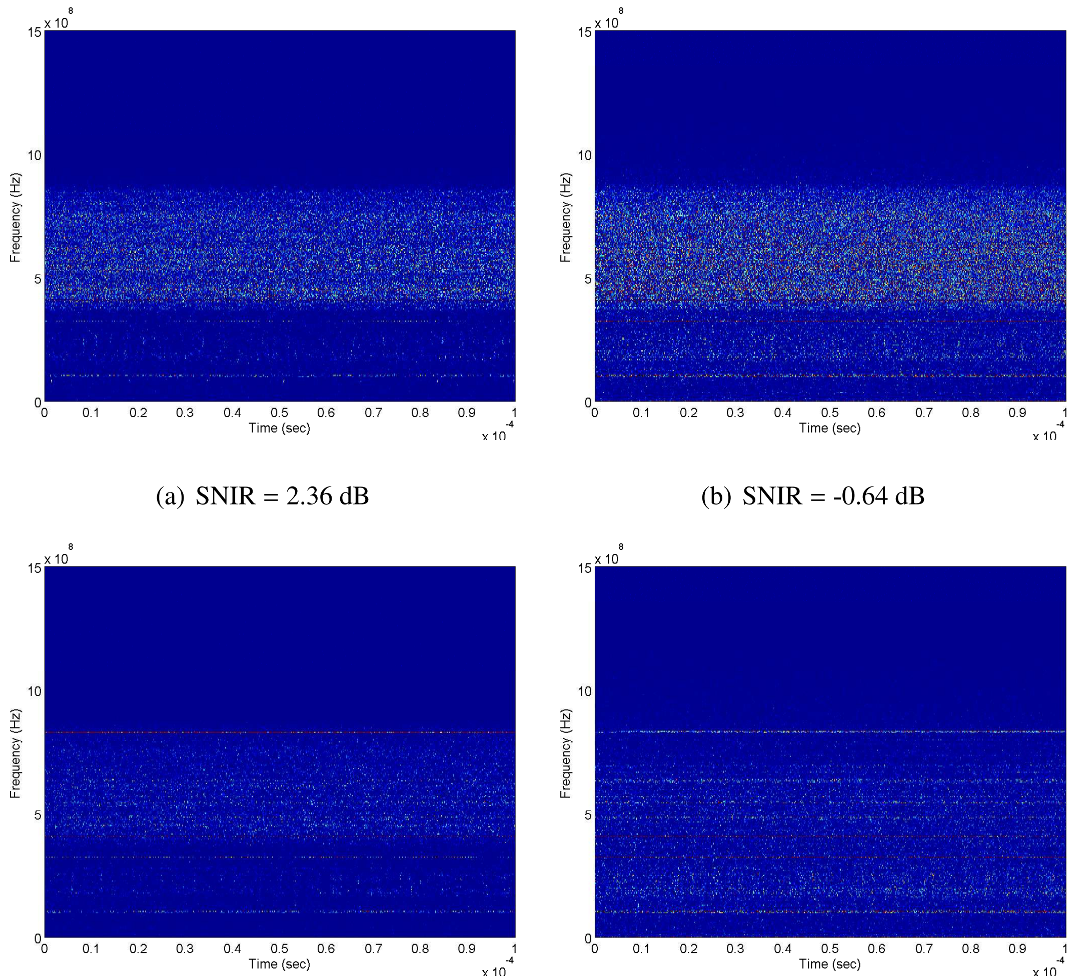

(a) SNIR = 2.36 dB

(b) SNIR = -0.64 dB

(c) SNIR = -3.64 dB

(d) SNIR = -21.64 dB

Figure 4.14: Analog source transmitted waveform QMFB layer 9 color plots at approximately various SNIR

plot in Figures 4.14 & 4.15 to show the increase in amplitude from the background measurement. There is banding evident in both Figure 4.14 and in the digital captures shown in Figure 4.15. This banding in frequency is due to the frequency coloring from

the log periodic antenna (LPA) antennas. Figures 4.14(b) & 4.14(c) there is an area in the middle of the plot where the bandwidth of the transmission can be determined. The actual bandwidth is much more difficult if not impossible to accurately predict in Figure 4.14(d). This is attributed to the lower transmission power level that is being sent to through the antenna. The power within the antenna passband (400 - 1000 MHz) is approximately the same power that is seen outside of the passband, creating the allusion that there is more bandwidth than what is actually being transmitted.

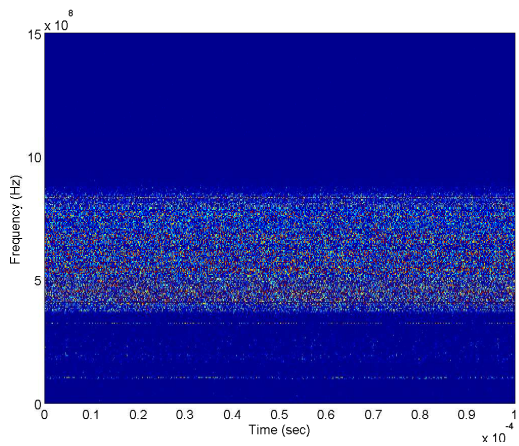

(a) SNIR = 5.97 dB

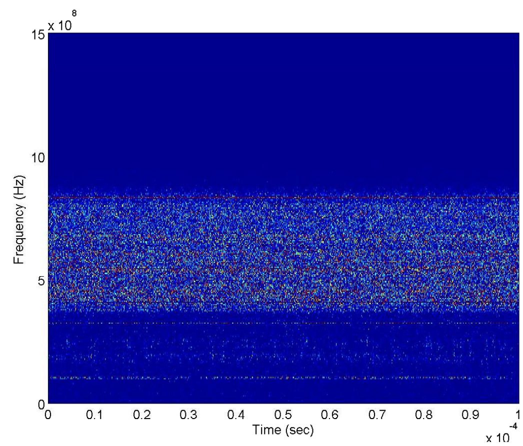

(b) SNIR = 2.97 dB

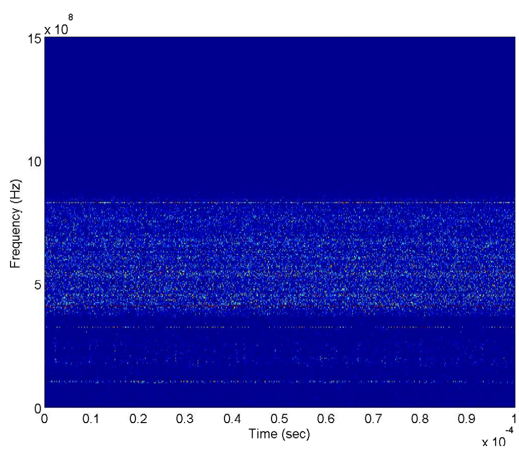

(c) SNIR = -0.03 dB

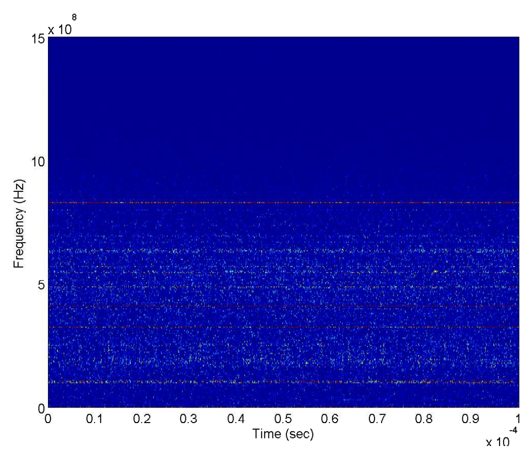

(d) SNIR = -18.03 dB

Figure 4.15: Digital source transmitted waveform QMFB layer 9 color plots at approximately various SNIR

The same frequency banding phenomenon that was seen in the analog transmitted signal is seen in the digital transmission. Additionally Figure 4.15(d) shows the same apparent increase in bandwidth as was seen in the analog transmission. By increasing removing the filters and therefore increasing the bandwidth of the system, the bandwidth might be able to be masked.

4.4.3 Cyclostationary Spectral Analysis.

The last attempt to determine useful parameters from an LPI waveform is the cyclostationary analysis. As explained in Chapter 3, the cyclostationary analysis will determine bandwidth and any repetition within the intercepted waveform. In this section the analog and digital source transmission that has been intercepted will be presented side by side. The analog transmission is the baseline for each of the digital transmissions. To make a fair comparison between the analog source and the digital source the capture where the analog source transmission SNIR equal to -0.64 dB plot will be compared with the digital sourceSNIR equal to -0.03 dB plot. This will facilitate a more useful comparison as seen in Figure 4.16. Banding is seen in both the analog and digital source transmissions, this is attributed to the antenna coloring the frequency spectrum. To get a better look at

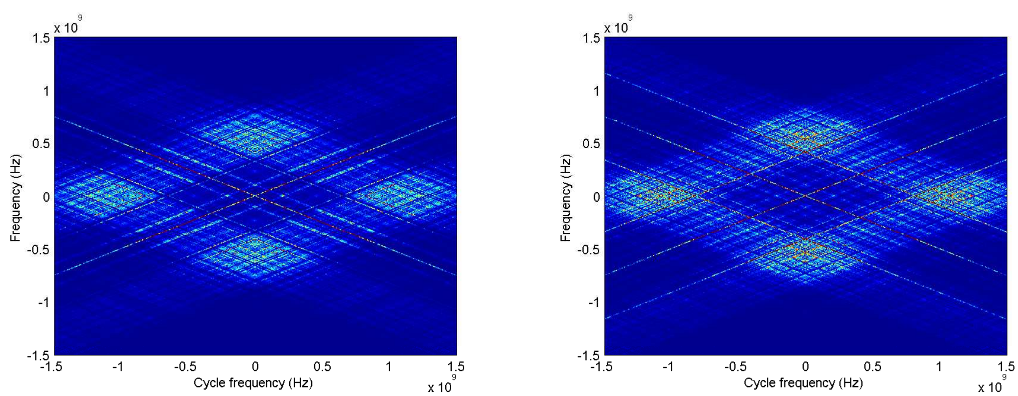

(a) Analog source at SNIR = -0.64 dB (b) Digital source SNIR = -0.03 dB

Figure 4.16: Analog and digital source transmitted waveform cyclostationary process

the analysis, the top quadrant of Figure 4.16 will be used to determine if there are useful parameters, as seen in Figure 4.17. While there is a slightly higher amplitude in the digital

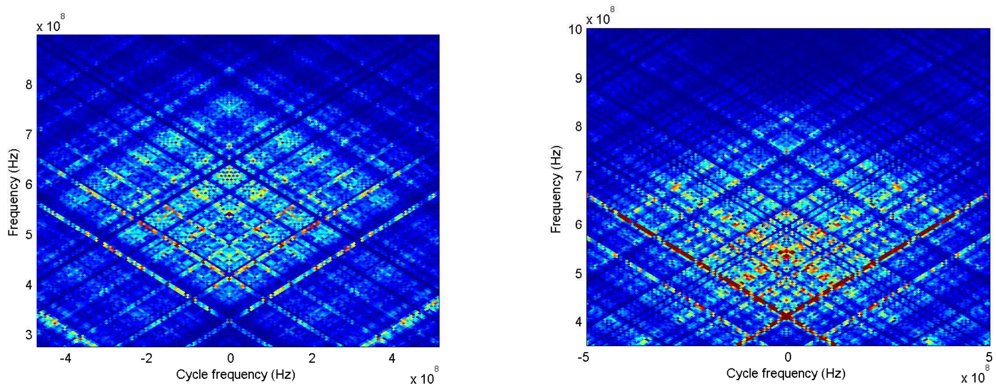

(a) Analog source SNIR = -0.64 dB

(b) Digital source SNIR = -0.03 dB

Figure 4.17: Analog and digital source transmitted waveform cyclostationary process top quadrant

source transmission, there are no extractable parameters. All the peaks that are seen in Figure 4.16(b) do not match with any of the known digital signal characteristics. However, some peaks might be due to individual groups of letters that repeat themselves within the transmitted message. This is purely an observation and has not been verified. The focus of this research was to determine if any parameters of a transmitted message could be calculated. In Figure 4.16(b), there are no extractable parameters as seen in Figure 4.17(b) other than bandwidth that has already been extracted using the QMFB analysis. For completeness, the analog and digital transmissions with the lowest SNIR are shown in Figure 4.19. These plots are very similar, and as the previous analysis at higher SNIRs indicated there is no information to be gained from the transmission signal.

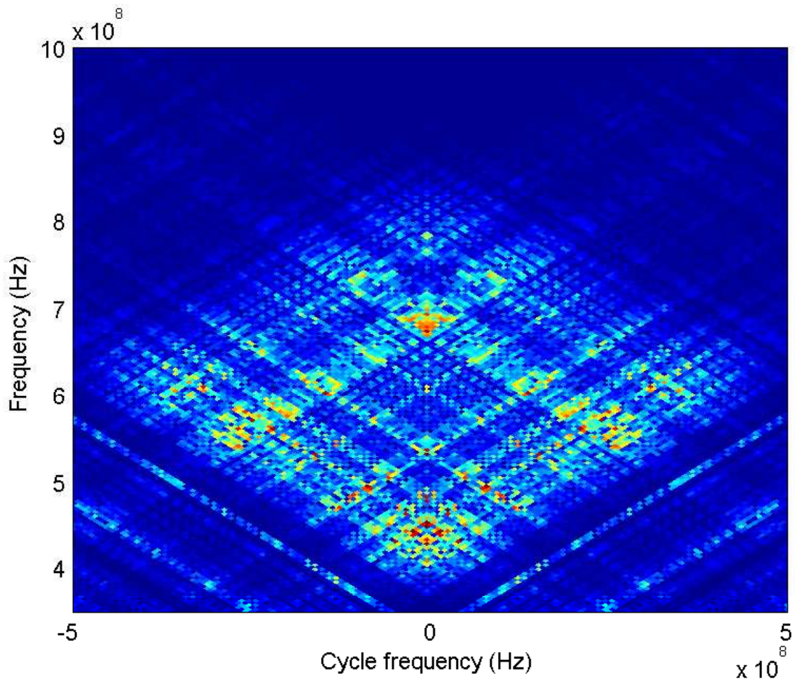

Figure 4.18: Digital source transmission cyclostationary analysis at SNIR = 5.97 dB zoomed in on top quadrant, with the color axis adjusted to better view features

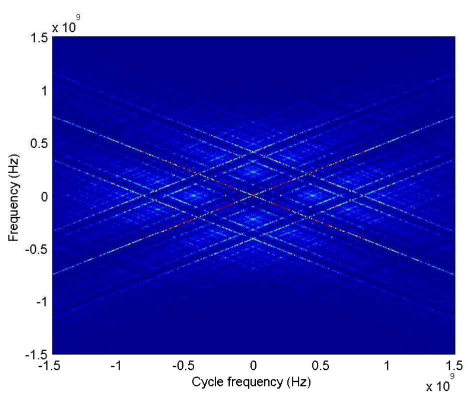

(a) Analog source

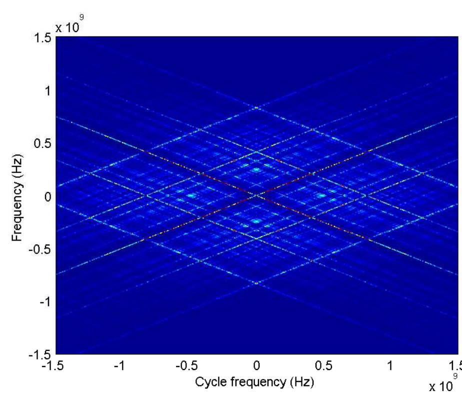

(b) Digital source

Figure 4.19: Analog and digital source transmitted waveform cyclostationary process at SNIR equal to -24 dB

4.5 Communication

It has been established that radar parameters are difficult to extract from signal strengths less than 0 dB SNIR. The next analysis is to determine the ability to decode the digital transmission. As discussed in Chapter 2, the waveform is an WGN waveform, and it will only correlate with an exact replica of itself; therefore communication can be accomplished if the transmitted waveform is known. Additionally, the error rate concepts of communication theory can be applied. Unlike traditional communication where symbol estimation which is done with power spectral density (PSD) estimation, the RNR waveform symbol estimation is done by correlating the received signal with a set of previously defined templates. Then the template with the highest correlation is estimated to be the transmitted template as explained in Chapter 3.

First, a simulation was performed to determine the SER with a template length of 1 μs and 128 templates. This simulation was accomplished to provide a baseline expectation for communication using a noise waveform. During the simulation, a set of templates were generated then each template was “transmitted” over an WGN channel and “received” using a correlation receiver. The SNIR was initially set at 10 dB, and each subsequent run of the simulation the SNIR was decreased by 5 dB steps until the SNIR was approximately -60 dB. Figure 4.20 shows the results of the simulation. An interesting observation from the simulation is the SER is zero until below -15 dB SNIR.

The next step was to perform the hardware experiment outlined in Chapter 3 for the SER. Figure 4.21 is a plot of the results obtained during the SER experiment.

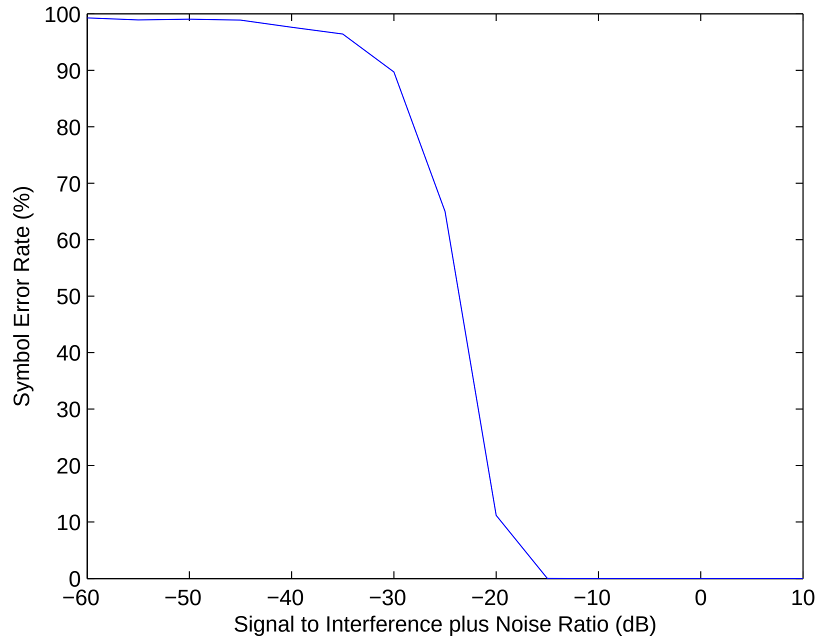

Figure 4.20: Simulated symbol error rate for digital noise waveform with 128 templates at a length of 1μs

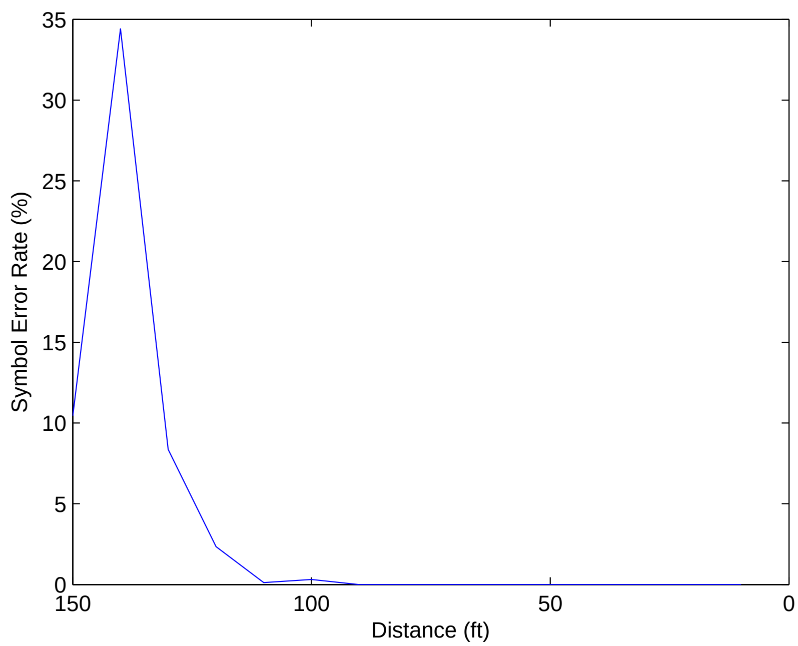

Figure 4.21: Symbol error rate hardware experiment results from 0 to 150 ft with a transmitted message "Hello World. This is a test message" repeated 28 times at each distance

At each distance, approximately 1000 symbols were transmitted. To achieve a more accurate SER, many more symbols would need to be transmitted. At several distances there were people who had walked down the hallway; at those distances the experiment was ran again in the event that the SER would not be accurate. However, at those distances the SER was not significantly impacted. For the distances up to 100 ft there were no errors, even when there was pedestrian traffic in the hallway.

4.6 Chapter Conclusion

In this chapter, the modifications to the system were analyzed to ensure that the current system with the modifications operated similarly to the previous system. The next step was to compare the digitally generated waveform to the analog waveform. The analysis showed that the digital waveform is similar and performed the radar functions the same as the analog source. The autocorrelation revealed some periodicity within the captured signal; however, this is due to the message being repeated. By not allowing the digital waveform generator to repeat its transmission this parameter would be eliminated. The other analysis did not reveal any information from the digital waveform other than bandwidth of the radar signal, which was also visible when the analog source was being used. Finally, in the communication test the experimental SER verifies the simulated SER; therefore, the simulated SER can be used to predict SER for the system at various distances in an indoor environment.

V. Conclusion

5.1 Chapter Overview

This research focused on implementing a digital waveform generation capability to enhance the Air Force Institute of Technology (AFIT) random noise radar (RNR). This increase in capability will further facilitate user generated waveform diversity and enabling digital communication over the noise waveform. In this chapter, an overview of the methodology is presented, and the results and contributions of this work are discussed. Additionally, proposed future work is detailed and listed to facilitate future research and development.

5.2 Review of Methodology

This research was conducted using a crawl, walk, run approach. First, the AFIT RNR system was modified to include the hardware components necessary to implement the digitally generated waveforms. Additionally, several hardware and software modifications were made to improve the flexibility of the AFIT RNR. After system modifications, it needed to be tested to ensure the modifications did not impact RNR functionality. The tests included an investigation of output frequency spectrum and a ranging function experiment. Next, the analog and digital waveforms were compared to ensure that the digital source transmission was similar to the analog source transmission. The main objective was to encode information onto a noise waveform while ensuring the low probability of intercept (LPI) properties of a truly random waveform were maintained. To achieve this objective, the analog and digital transmissions needed to be measured and analyzed using LPI detection tools. These LPI tools provide a qualitative visual assessment as to the ability to extract parameters from the received signal. Finally, the

digital communication effectiveness was measured, with hardware symbol error rate (SER) calculated and compared to simulated SER.

5.3 Results and Contributions

The RNR system modifications were successful in implementing the digital waveform generator. By including switches and attenuators into the system to increase the total flexibility, the analog source took about a 5 dB decrease to output power compared to the original system. However, the through losses from the switches and the amplifier provide an output power from the digital source that is approximately equal to the previous AFIT RNR. Furthermore, the analog and digital sources provide the same ranging capability. This was very important to ensure that the original operation of the AFIT RNR was not fundamentally changed. When not repeatedly transmitting the same message, the LPI characteristics of the digital source match that of the analog source. To increase the RNR effectiveness it may be advantageous to repeatedly transmit the message. Therefore, a sufficient encoding technique needs to be developed to allow the transmission to be repeated without using the same templates. As shown in this research, the digitally generated waveform using a simple one to one encoding of American Standard Code for Information Interchange (ASCII) characters to templates is an effective way to digitally encode data on a RNR waveform and maintain the LPI characteristics of an analog generated waveform. Additionally, using the noise waveform to communicate over a large distance with a low power radar signal was shown to be effective.

The contributions of this work will facilitate use of the AFIT RNR in low probability of detection (LPD) communication and radar. Furthermore, the AFIT RNR as currently designed can be used for many applications other than RNR. This new platform will be able to facilitate research in baseband waveform creation for use in both radar and communication applications.

5.4 Future Work

At the conclusion of this research, there are many applications that have just had the surface scratched, leaving many opportunities for future research in the RNR and communication fields. The proposed research areas listed here are from the many routes that have been seen during the research into encoding information onto a noise waveform. Suggested future opportunities for research include:

- Further verify the simulated symbol error rate by performing the symbol error rate experiment outside with approximately 100,000 transmitted symbols.

- Explore current low probability of intercept detection techniques to determine if radar parameters are able to be extracted.

- Research encoding techniques to improve the speed at which information can be transmitted over the noise waveform.

- Investigate ways to increase the speed of acquisition of transmitted and received waveforms.

- Investigate techniques to implement the digital source and template replay approach into the navigation algorithm.

Appendix A: Additional Figures

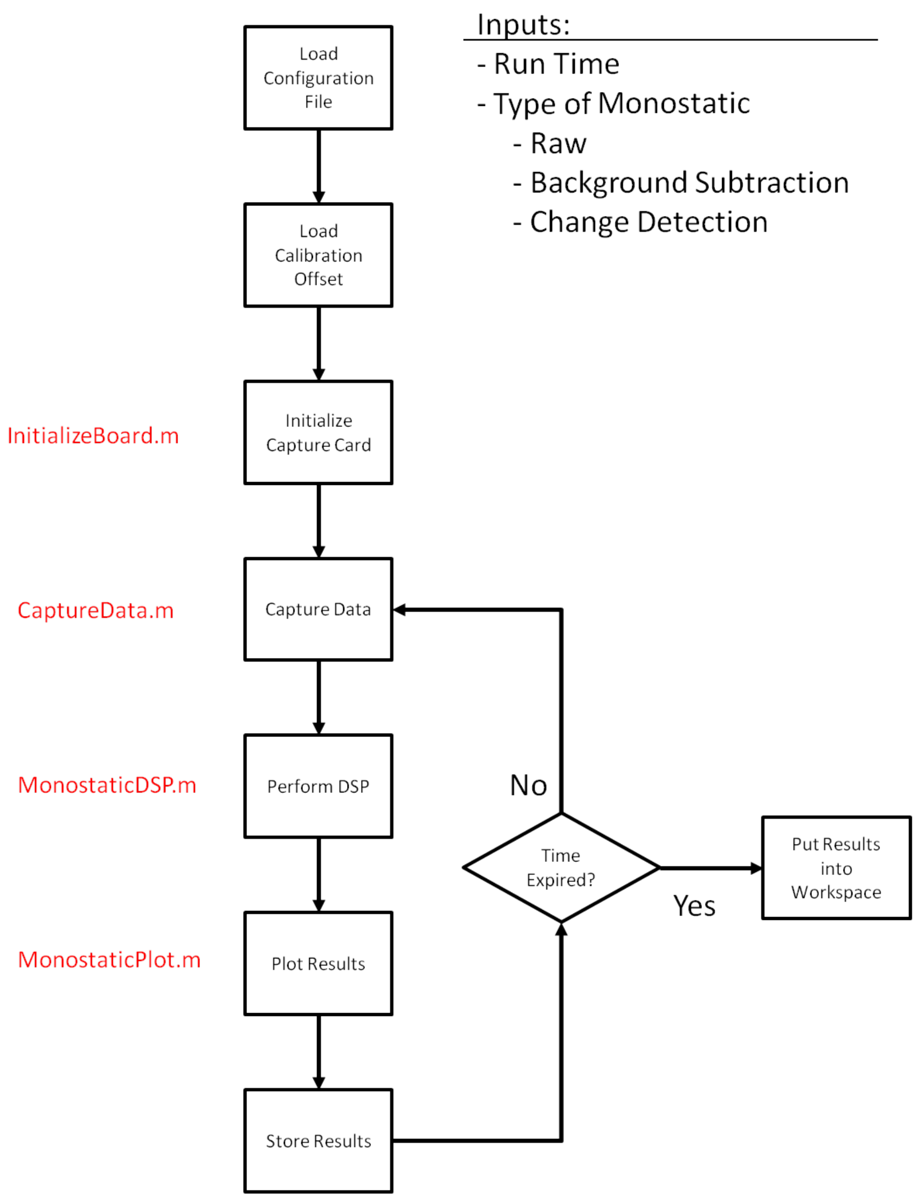

Figure A.1: Flow diagram of NoNET Monostatic radar routine

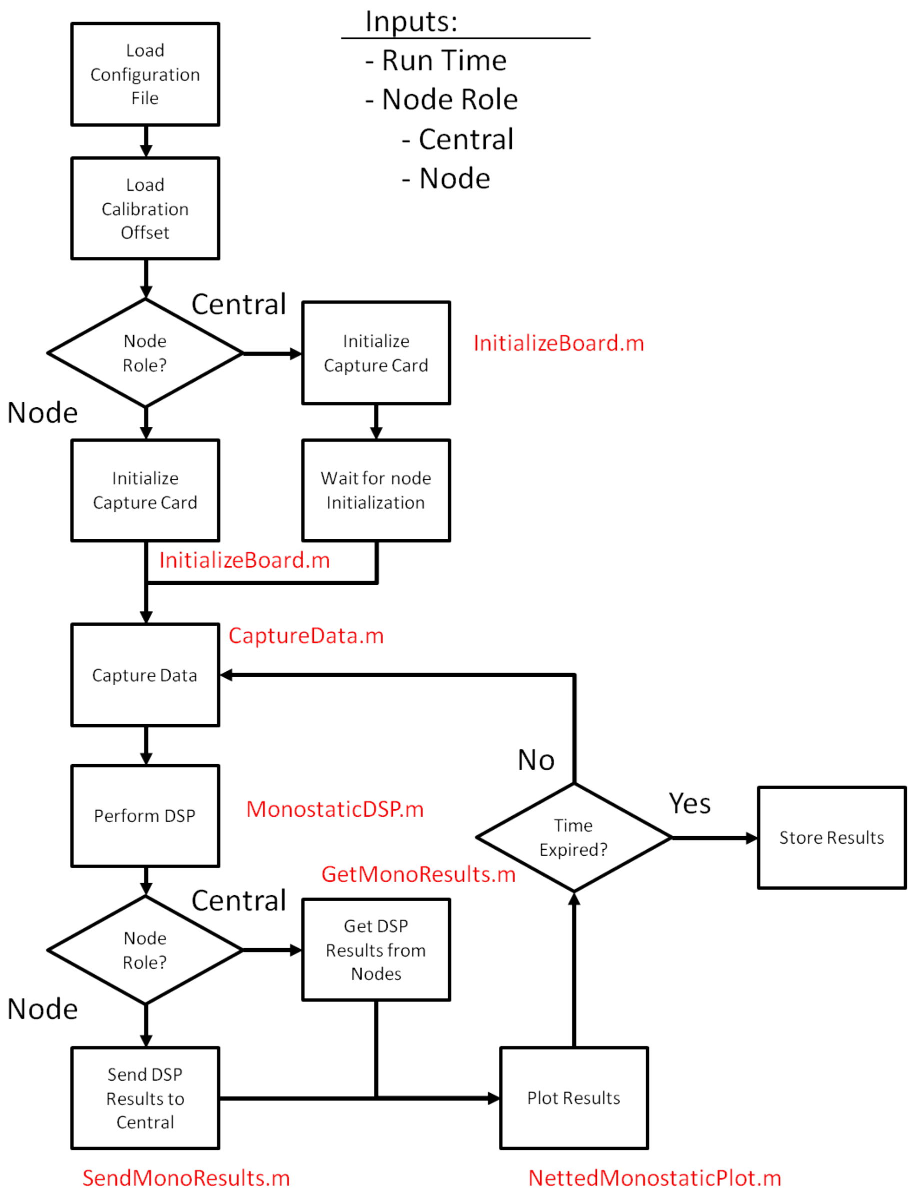

Figure A.2: Flow diagram of NoNET netted monostatic radar routine

Appendix B: Additional research

This appendix will detail additional research that was conducted and any other research efforts that was not included in the thesis. These experiments were either non-conclusive or did not contribute to the research. The purpose of including these efforts is to detail the full extent of the research and for archival purposes. In this appendix each section will detail a research effort with the methodology, graphs or plots and some analysis, and a conclusion.

B.1 IRA development and test

B.1.1 Components.

The impulse radiating antenna (IRA) as seen in Figure B.1 consists of an aluminum dish, double sided copper plated FR4, 200 Ω resistors, approximately 100 Ω RF cable, ferrite beads, and a 50 Ω to 100 Ω splitter (Balun).

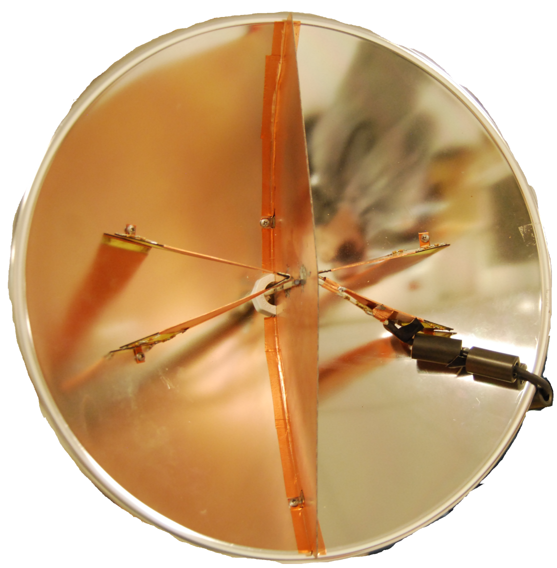

Figure B.1: AFIT developed IRA based on Baum and Farr designs [2]

This design is based on previous designs by Baum and Farr except at lower frequencies and much lower power [2]. The FR4 wave launchers are designed based on mathematical equations detailed in Farr's many published papers. These equations were incorporated into a matlab script in which an engineer can make trade-offs to determine the best design for the IRA.

B.1.2 IRA Design Considerations.

By using the matlab script function IRADesign and inputing the diameter of the dish, the depth of the dish, and the required feed arm resistance the design of the feed arms and the placement of the arms on the dish are determined. This matlab function is based on the published papers by Farr. The matlab function is a starting point and could be improved by adjusting angles or adding a ground plane down the middle of the dish. There are many papers listed on Farr-research.com that detail the different designs of the IRA.

B.1.3 Conclusion and Future Work.

The IRA might be a promising antenna for use with the Air Force Institute of Technology (AFIT) random noise radar (RNR). However, a more in depth design and a detailed analysis of the antenna pattern and response is needed. A larger antenna might be more successful for lower frequencies. Additionally, there are many new IRA designs from FARR Research that should be analyzed and incorporated into a final design.

B.2 Antenna comparison

The antenna comparison experiment was to compare several different antenna designs that might be used in the AFIT RNR. Three antennas were being considered. The log periodic antenna (LPA) antenna that was included in the original design, an antenna designed by a previous AFIT masters student [10], and a small IRA design based on work by Baum and Farr [2].

B.2.1 Methodology.

The setup of this experiment consisted of the AFIT RNR transmit output was connected to the antenna under test (AUT). The receiver input was connected to a dipole antenna. This dipole antenna is a SMA bulkhead connector from Fairview Microwave part number SC3730 and is shown in Figure B.2. The AUT and the dipole antenna were setup

Figure B.2: SMA connector used as a dipole antenna

up 6 ft apart, Figure B.3 shows the setup of this experiment in the microwave lab. For each antenna setup the transmit and receive filters are switched to get all configurations, these configurations and test matrix is shown in Table B.1. The captured data is then post-processed using AFIT LORE Processing INtegrated Environment (ALPINE) developed at AFIT specifically for use with radar cross-section (RCS) and RNR data. Within ALPINE there is a readNoNET script that pulls in the data in the NoNET format and converts it to the format needed for processing with the other ALPINE tools. The cross correlation between the transmit and received waveforms is the impulse response that ALPINE uses to determine the frequency response.

B.2.2 Results and Analysis.

Figure B.4 shows the calculated LPA frequency spectrum. These results are averaged over 20 captures to decrease the noise in the final results. In Figure B.4(a) the LPA lower cutoff can be seen at 400 MHz. These results are consistent with the measured results in Thorson's plot seen in Figure B.5. Notice the null around 550 MHz in both Figure B.4(a) & B.5.


Figure B.3: Experiment setup for antenna comparison

Table B.1: Antenna Characterization Test Matrix

Antenna	Transmit Filter	Receive Filter
LPA	ON	ON
LPA	ON	OFF
LPA	OFF	ON
LPA	OFF	OFF
IRA	ON	ON
IRA	ON	OFF
IRA	OFF	ON
IRA	OFF	OFF
Vivaldi	ON	ON
Vivaldi	ON	OFF
Vivaldi	OFF	ON
Vivaldi	OFF	OFF

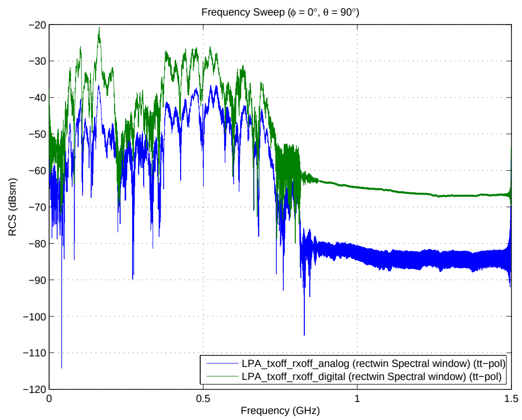

(a) Transmit filters off, received filters off

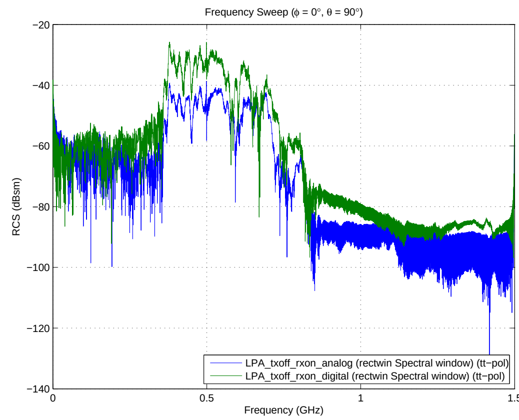

(b) Transmit filters off, received filters on

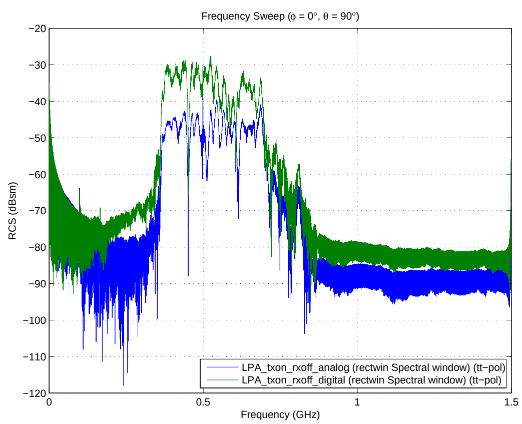

(c) Transmit filters on, received filters off

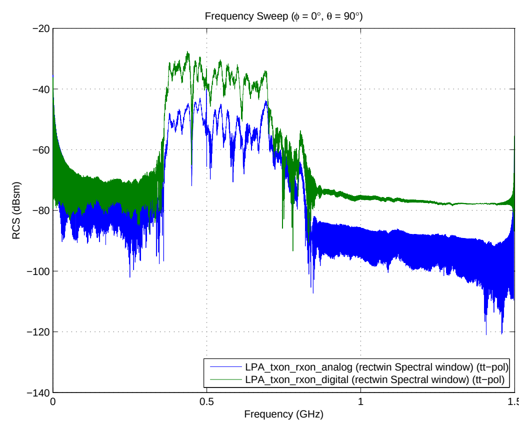

(d) Transmit filters on, received filters on

Figure B.4: LPA antenna comparison

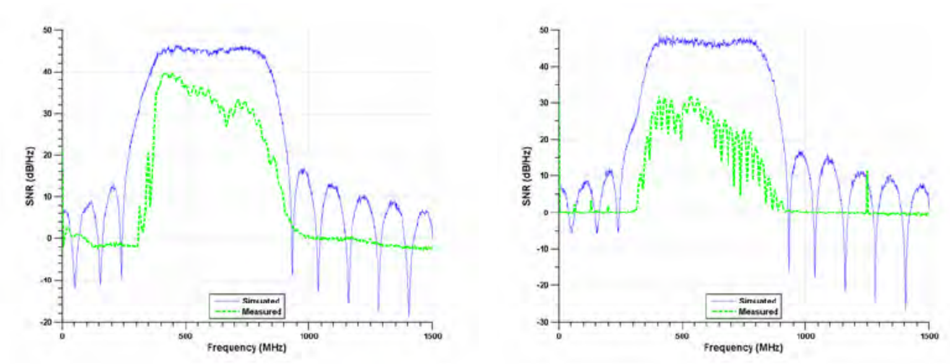

(a) (b)

Figure 4.17. A comparison between the simulated and measured pre-processing SNR as a function of frequency is made using (a) the standard AFIT RNR configuration and (b) the horn-modified configuration. Target at 6 meters, HH polarization.

Figure B.5: LPA measurement from Thorson Thesis [23]

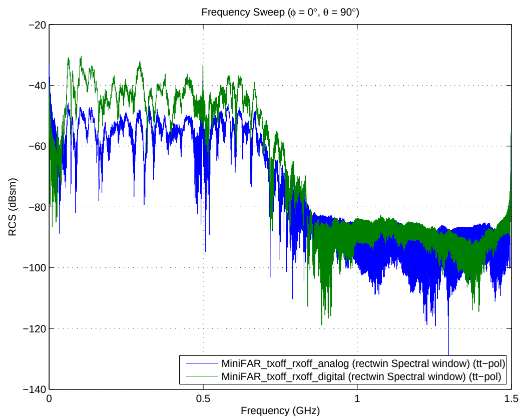

(a) Transmit filters off, received filters off

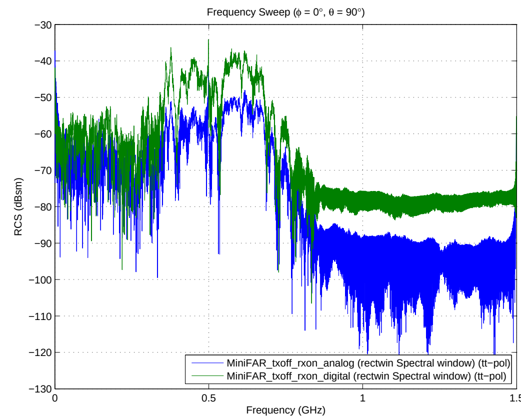

(b) Transmit filters off, received filters on

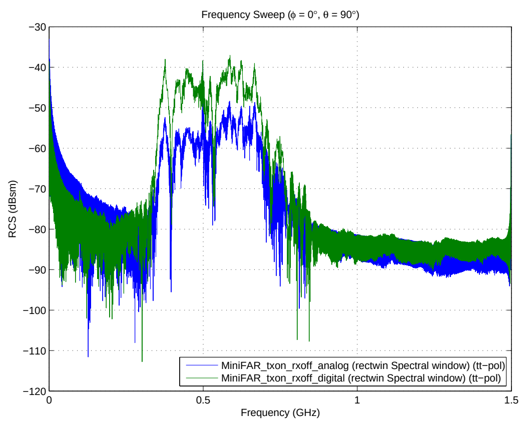

(c) Transmit filters on, received filters off

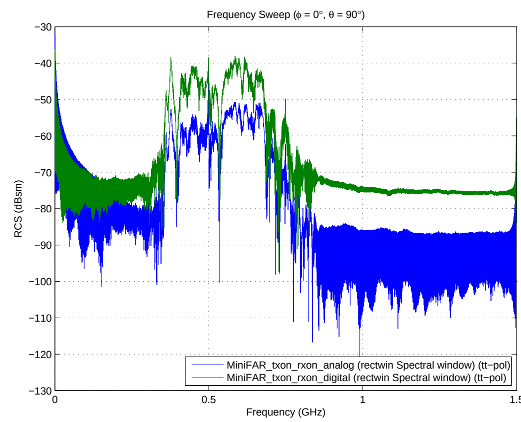

(d) Transmit filters on, received filters on

Figure B.6: IRA antenna comparison

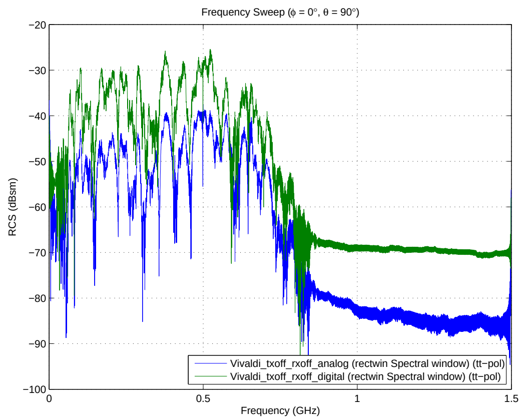

(a) Transmit filters off, received filters off

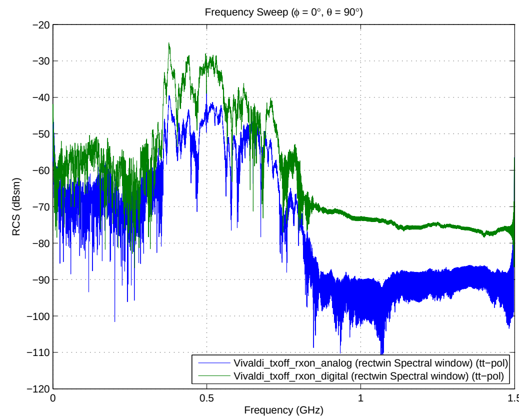

(b) Transmit filters off, received filters on

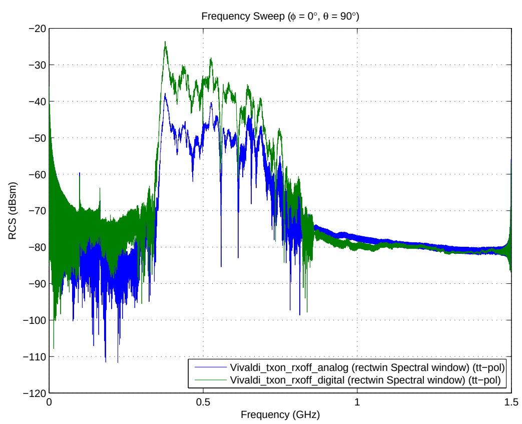

(c) Transmit filters on, received filters off

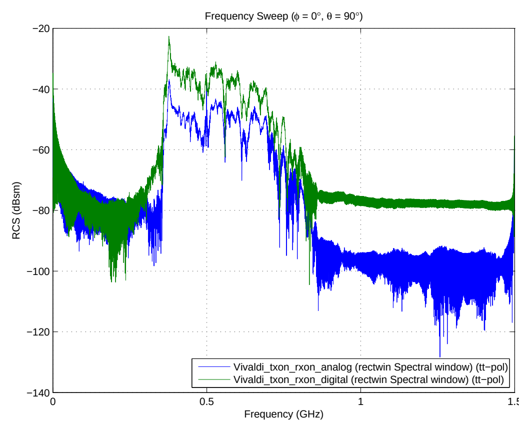

(d) Transmit filters on, received filters on

Figure B.7: Vivaldi antenna comparison

Figure B.8 & B.9 show a comparison of each antenna. From these plots there is very little difference between antennas, which was not expected.

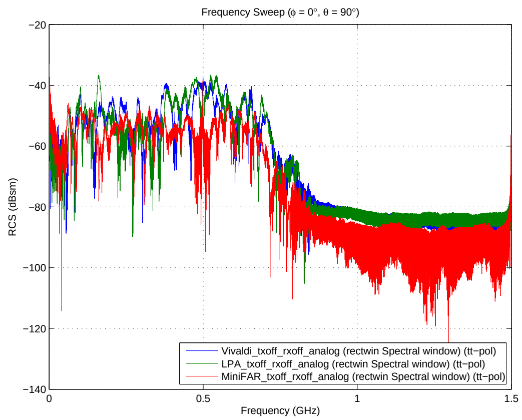

(a) Transmit filters off, received filters off

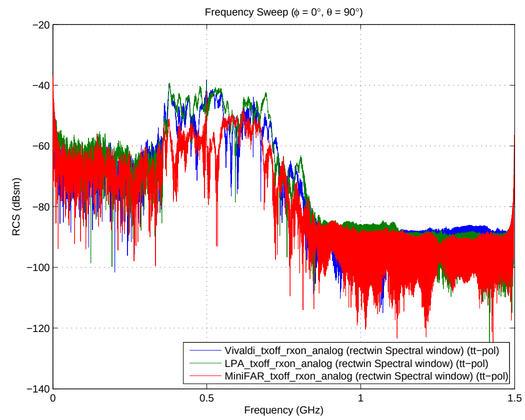

(b) Transmit filters off, received filters on

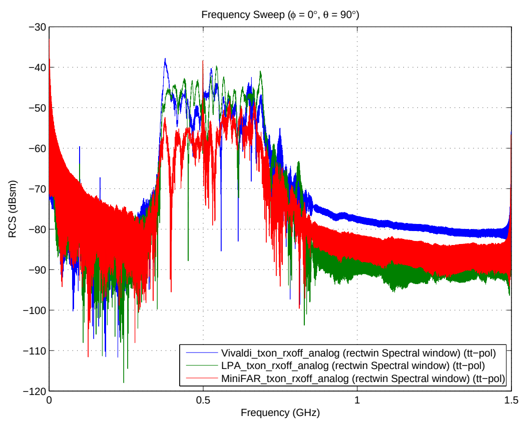

(c) Transmit filters on, received filters off

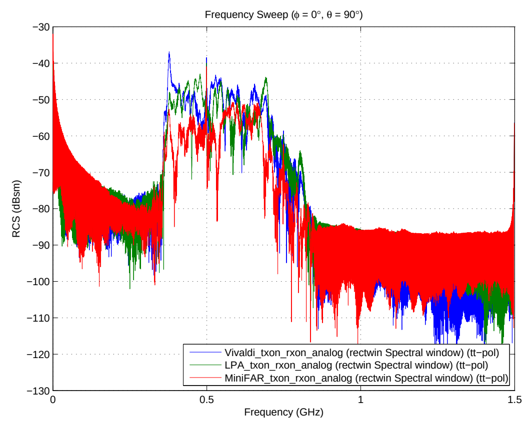

(d) Transmit filters on, received filters on

Figure B.8: Antenna comparison using analog source

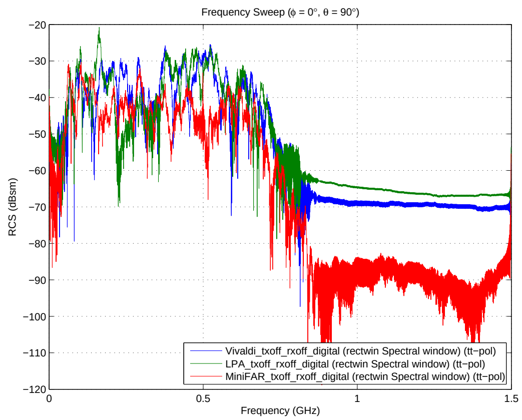

(a) Transmit filters off, received filters off

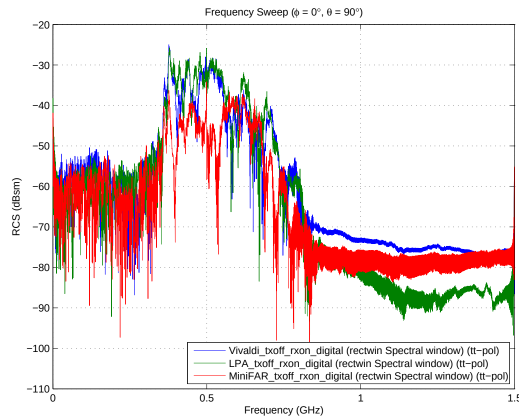

(b) Transmit filters off, received filters on

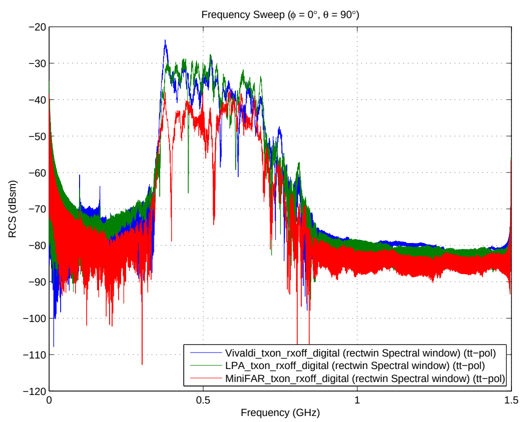

(c) Transmit filters on, received filters off

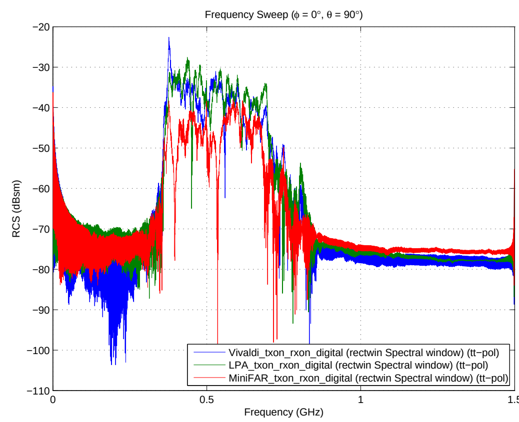

(d) Transmit filters on, received filters on

Figure B.9: Antenna comparison using digital source

B.2.3 Conclusion.

After analyzing the results of the antenna comparison test, it was determined that further research needed to be accomplished on the IRA. This is primarily due to the results shown here did not match what was seen on the network analyzer. The results from the network analyzer were not captured and saved, but were just observed. After this experiment it was determined that the IRA was not operating in the desired frequency range. Therefore, further experimentation and analysis is needed to optimize the IRA for use with the AFIT RNR.

B.3 Matlab IRADesign function

```
function [alpha1, beta1, beta2, focus] = IRADesign(D,d, resistance)
%===========================================================================
% EENG 627 - Final Project
% Capt Aaron Myers
% 20 August 2012
%
% This script will calculate the parameters associated with IRA design.
% Based on the papers presented on Farr-research's website.
%
%   IRADesign(D,d, resistance)
%
%   Inputs - D - diameter of the dish in meters
%          - d - depth of dish from rim to bottom of parabola in meteres
%          - resistance - required feed arm resistance
%
% Author - Capt Aaron Myers 20 Aug 12
% Updated - Capt Josh Hardin 08 Mar 13
%===========================================================================

% Constants
e0 = 8.854187817620e-12; % F/m
u0 = 4*pi*1e-7; % N/A2
z0 = sqrt(u0/e0); % ohms

% Dish Parameters
focus = D^2/(16*d);
fd = focus/D;

% Feed Arm Resistance
```

```
z = 400;
fg = z/z0;
m = 0.001:.001:.999; %fg = ellipke(m)/ellipke(1-m)
y = @(m)ellipke(m)./ellipke(1-m);
m1 = fzero(@(m)y(m)-fg, .5);  %# find solution near x=-10

% Feed Arm Angles - Development of IRA Reflector, partI
beta = atan(1/(2*fd-1/(8*fd)));
beta1 = 2*atan(m1^(.25)*tan(beta/2))*180/(pi);
beta2 = 2*atan(m1^(-.25)*tan(beta/2))*180/(pi);
alpha = 2.*atan(m.^(-.25).*tan(beta./2)).*180./(pi)-...
    2.*atan(m.^(.25).*tan(beta./2)).*180./(pi);

fg = z0.*(ellipke(m)./(2.*ellipke(1-m)));

indx = find(resistance*.999 < fg & fg < resistance*1.001,1);

alpha1 = alpha(indx);

x = -D/2:.0001:D/2;
y = (d/((D/2)^2)).*(x).^2;

theta1 = linspace(0,beta1*(pi/180),100)-(pi/2);
rho1 = ones(1,100) *.03;
[xarc1,yarc1] = pol2cart(theta1,rho1);
xarc1 = xarc1 + 0;
yarc1 = yarc1 + focus;

theta3 = linspace(beta1*(pi/180),beta2*(pi/180),100)-(pi/2);
rho3 = ones(1,100) * .06;
[xarc3,yarc3] = pol2cart(theta3,rho3);
xarc3 = xarc3 + 0;
```

```
yarc3 = yarc3 + focus;

theta4 = linspace(-15*(pi/180),15*(pi/180),100);
rho4 = ones(1,100) * .06;
[xarc4,yarc4] = pol2cart(theta4,rho4);
xarc4 = xarc4 + 0;
yarc4 = yarc4 + 0;

h = figure;
subplot(1,2,1),hold on
subplot(1,2,1),...
    title('Side View'), xlabel('Distance (m)'), ylabel('Distance (m)')
subplot(1,2,1),xlim([(-D/2)*1.2 (D/2)*1.2])
subplot(1,2,1),ylim([0 (D/2)*1.75])
subplot(1,2,1),plot(x,y, 'k', 'linewidth', 3)
subplot(1,2,1),plot([0 focus*1.5* sind(beta1)], ...
    [focus focus - focus*1.5*cosd(beta1)],'r')
subplot(1,2,1),plot([0 focus*1.5* sind(beta2)], ...
    [focus focus - focus*1.5*cosd(beta2)], 'r')
subplot(1,2,1),plot([0 -focus*1.5* sind(beta1)], ...
    [focus focus - focus*1.5*cosd(beta1)],'r')
subplot(1,2,1),plot([0 -focus*1.5* sind(beta2)], ...
    [focus focus - focus*1.5*cosd(beta2)], 'r')
subplot(1,2,1),plot(xarc1,yarc1,'b')
subplot(1,2,1),plot(xarc3,yarc3,'b')
subplot(1,2,1),...
    text(focus*.40,focus*.6,['\beta_1 = ' num2str(beta1) ' degs'])
subplot(1,2,1),...
    text(focus*.95,focus*.95,['\alpha = ' num2str(alpha1) ' degs'])

subplot(1,2,2),hold on
subplot(1,2,2),...
```

```
    title('Top View'), xlabel('Distance (m)'), ylabel('Distance (m)')
subplot(1,2,2),xlim([(-D/2)*1.2 (D/2)*1.2])
subplot(1,2,2),ylim([(-D/2)*1.2 (D/2)*1.2])
subplot(1,2,2),plot(x,sqrt((D/2).^2 - x.^2) , 'k', 'linewidth', 3)
subplot(1,2,2),plot(x,-sqrt((D/2).^2 - x.^2) , 'k', 'linewidth', 3)
subplot(1,2,2),plot([0 (D/2)*cosd(15)], [0 (D/2)*sind(15)],'r')
subplot(1,2,2),plot([0 (D/2)*cosd(15)], [0 -(D/2)*sind(15)], 'r')
subplot(1,2,2),plot([0 -(D/2)*cosd(15)], [0 (D/2)*sind(15)],'r')
subplot(1,2,2),plot([0 -(D/2)*cosd(15)], [0 -(D/2)*sind(15)], 'r')
subplot(1,2,2),plot(xarc4,yarc4,'b')
subplot(1,2,2),plot(-xarc4,yarc4,'b')
subplot(1,2,2),text(D/4,0,'30 degs')
subplot(1,2,2),text(-D/2.5,0,'30 degs')
pos = get(h,'position');
pos(3:4) = [1004 419];
set(h, 'position', pos);
```

Appendix C: AFIT NoNET Users Manual

The purpose of this appendix is to detail the use of the Air Force Institute of Technology (AFIT) random noise radar (RNR) through the NoNET software. This appendix will cover the how to use the NoNET software to utilize the AFIT RNR in a monostatic mode in both the command line and from the graphical user interface (GUI). The GUI software is not complete and has random compability issues. The GUI provides a quick and dirty evaluation of the radar operation. The command line operations should be used for a more robust radar operation.

C.1 Power Up

To turn on the AFIT RNR either plug the power strip into the wall, or the AC/DC power inverter and turn on the inverter (Figure C.1). Next, turn the power

Figure C.1: Power strip plugged into AC/DC power inverter

strip (Figure C.2)and listen for the RNR box to power up. The fans inside the box should be audible. *****Wait 5-10 seconds to turn on the computer. This step is very important, if the computer is turned on before the RNR box the Peripheral Component Interconnect (PCI) cards will not be initialized properly and will not communicate with the computer.***** Now that the RNR unit is powerup, turn on the

Figure C.2: Power strip for AFIT RNR

computer (Figure C.3). After bootup, the windows splash screen will be displayed with the login prompts. Select the “User” user and enter the password obtained from the AFIT RNR custodian. After login, start matlab; matlab will open with the NoNET directory added to the matlab path and will be the defult directory. Here there are two choices for operating the AFIT RNR, either using the command line or by using the GUI.

Figure C.3: AFIT RNR Computer

C.2 NoNET GUI

Type “NoNET” into the matlab command prompt. The GUI will display (Figure C.4). The configuration of the AFIT RNR is controlled by the tabs labeled “Control”, “Acq

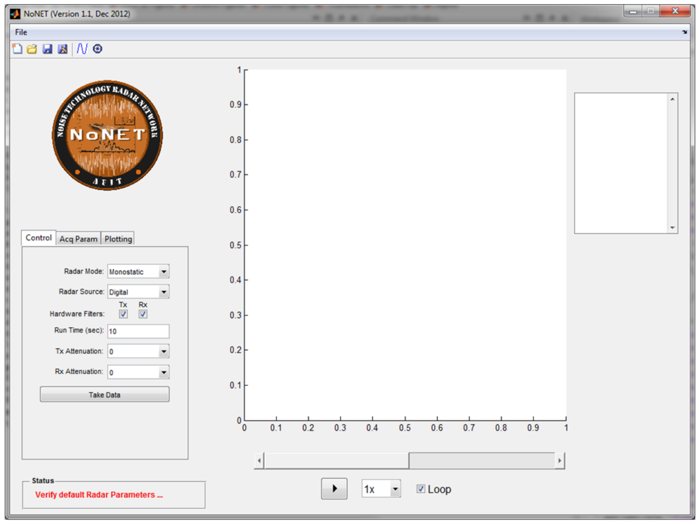

Figure C.4: NoNET GUI

Param", and "Plotting". The "Radar Mode" drop down box only works for Monostatic and Calibrate modes. The other modes listed are not connected to a specific NoNET routine.

Select the desired "Radar Source" (Figure C.5), the options are analog or digital. If

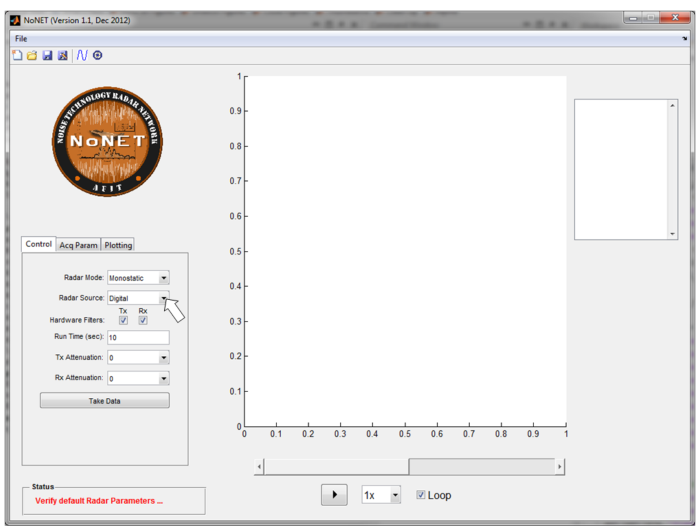

Figure C.5: NoNET Radar source selection

selecting the digital source, the operator needs to load a waveform to the arbitrary waveform generator (AWG). This is done by clicking the AWG button (Section C.3). Next, check the

configurations on each of the tabs to ensure that the correct settings are used for the users application (Figure C.6) After verifying the configuration click the “Take Data” button.

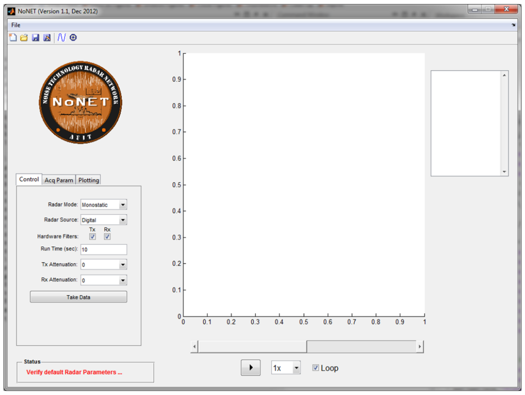

(a) Control Tab

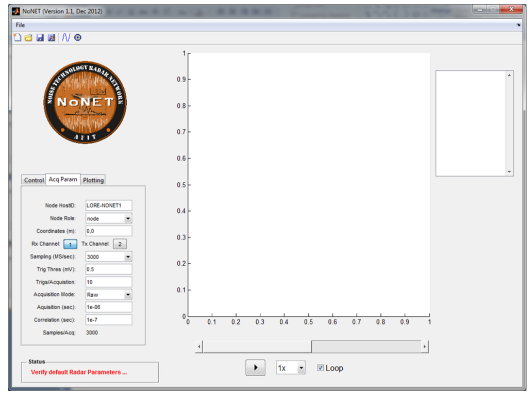

(b) Acquisition Parameters Tab

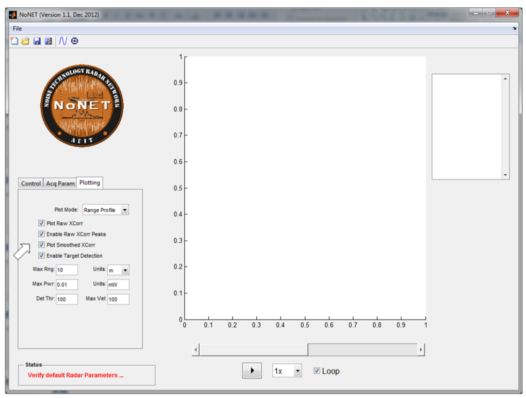

(c) Plotting Tab

Figure C.6: GUI configuration tabs

The status of the radar operation will be displayed in the “Status” window at the bottom of the GUI. Once the radar is operating the results will be displayed on the plot to the right of the configuration tabs. Once the radar operation is complete the results will be saved in the far right window. This allows for play-back of previous radar operations. To save a specific radar operation data collection, use the “File” drop down menu.

C.3 AWG GUI

This section describes how to load a waveform into the AWG using the AWG GUI (Figure C.7). The AWG GUI will open and allow the user to load a desired waveform

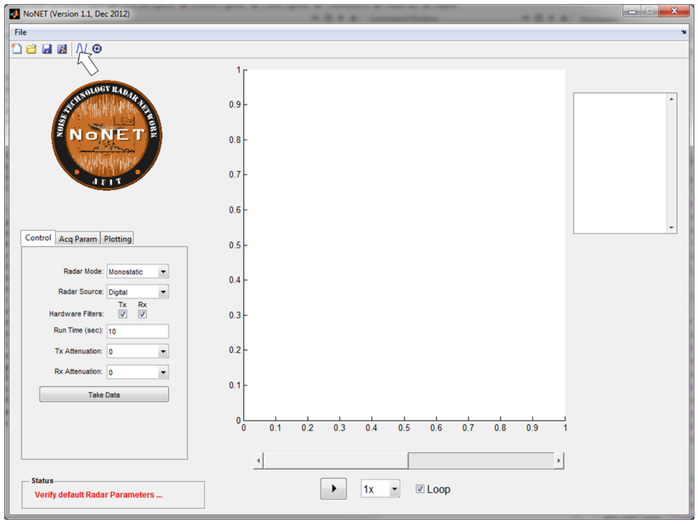

Figure C.7: Open AWG GUI

into the AWG (Figure C.8). The icons in the menubar to the left of the divider control

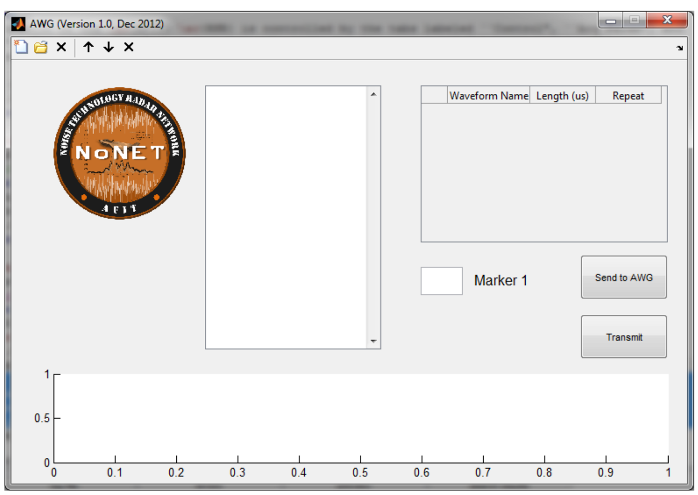

Figure C.8: AWG GUI

the waveforms that are loaded into the GUI, the icons to the right of the divider control the

waveforms that have been selected to transmit (Figure C.9). Once the AWG GUI is open a

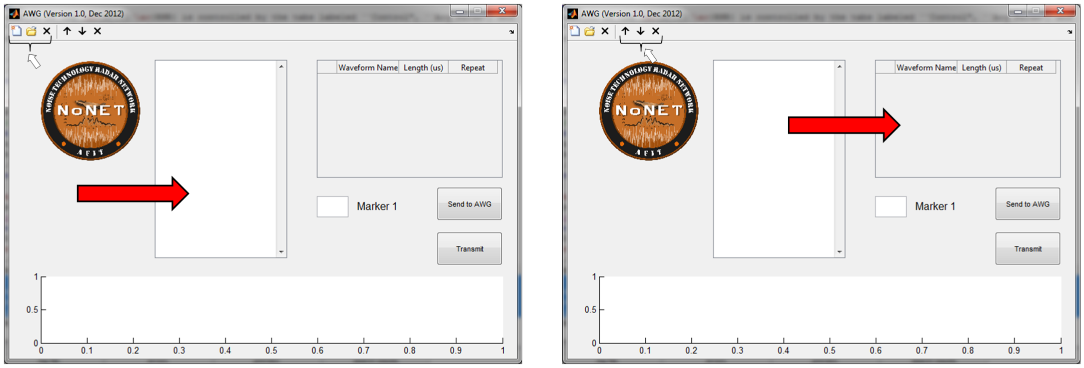

(a) Waveform loaded into GUI controls (b) Waveforms selected for transmit controls

Figure C.9: AWG GUI waveform controls

waveform needs to be loaded. To load a waveform into the AWG GUI click the open icon on the menu toolbar (Figure C.10). The user can select multiple waveforms to import into

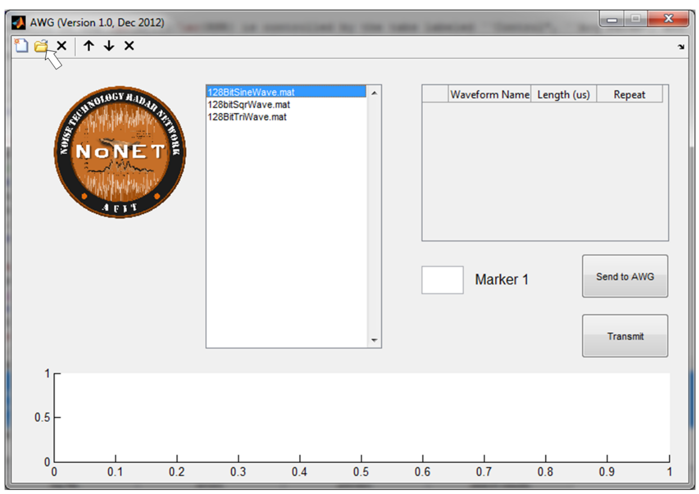

Figure C.10: Open a waveform in the AWG GUI

the GUI. Once imported into the GUI the waveforms will be listed in the window. To place them into the sequence to be transmitted double click the desired waveform. It will then be listed in the next window and displayed on the plot at the bottom (Figure C.11). If a

loaded waveform is to be repeated enter the number of repetitions in the repeat column, this will repeat the waveform and will be represented in the plot on the bottom. The plot at the bottom of the GUI is the waveform that will be loaded and transmitted. Now the user can

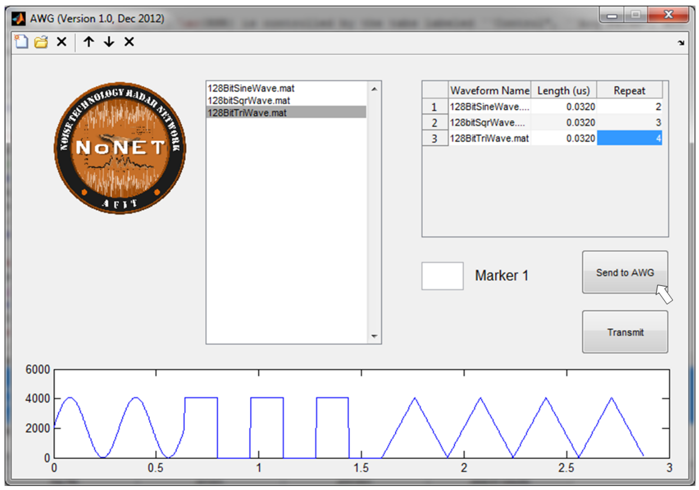

Figure C.11: Waveforms selected for transmission

select the "Send to AWG" button. Once the operation is complete the button will turn green. If the button turns red and error occurred and the waveform was not able to be loaded. Next, the user can hit the transmit button and the AWG will start a continuous looping transmission of the loaded waveforms. The AWG GUI window can now be minimized or closed (NOTE: If the window is closed the only way to stop the digital transmission is to load another waveform, open the AWG GUI and click the transmit button twice, or use the command line function "TransmitWaveform32(0)").

C.4 NoNET Command Line

To operate the NoNET software in the command line the user should type the requested function in the matlab command line window. The following section will detail the basic radar commands to perform a calibration, and a monostatic radar operation.

C.4.1 Calibration via Command Line.

To calibrate the NoNET radar at a specific location the user can either type “Calibrate” and follow the pop-up window prompts or type “Calibrate(range in meters)” (Figure C.12). The calibration routine will perform a background capture, then the user is asked to place the target into the scene (the target should be placed 3 - 5 m [17]). After the calibration routine is finished the calibration offset is stored in the calibrate.mat file under the ConfigurationFiles folder. The calibrate.mat file is called during the beginning of the radar operation.

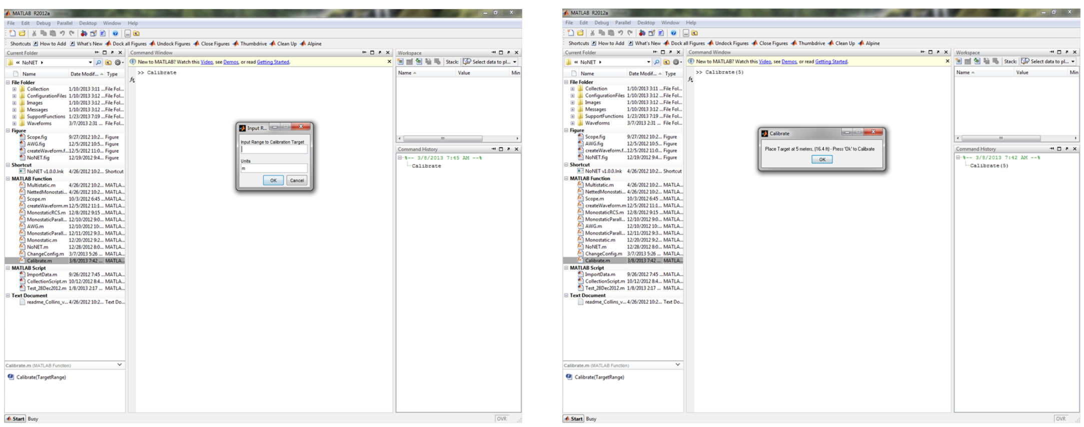

(a) Calibration using prompts

(b) Calibration using range entered in command line

Figure C.12: AFIT RNR Calibration

C.4.2 Monostatic radar operation via Command Line.

To operate the radar in monostatic mode, the user should first type “load(’config.mat’); config” to display the configuration file(Figure). All radar settings are based on the configuration file.

To change the saved configuration type “ChangeConfig(’current’)” into the matlab command prompt. This will save the current configuration to the config.mat file under

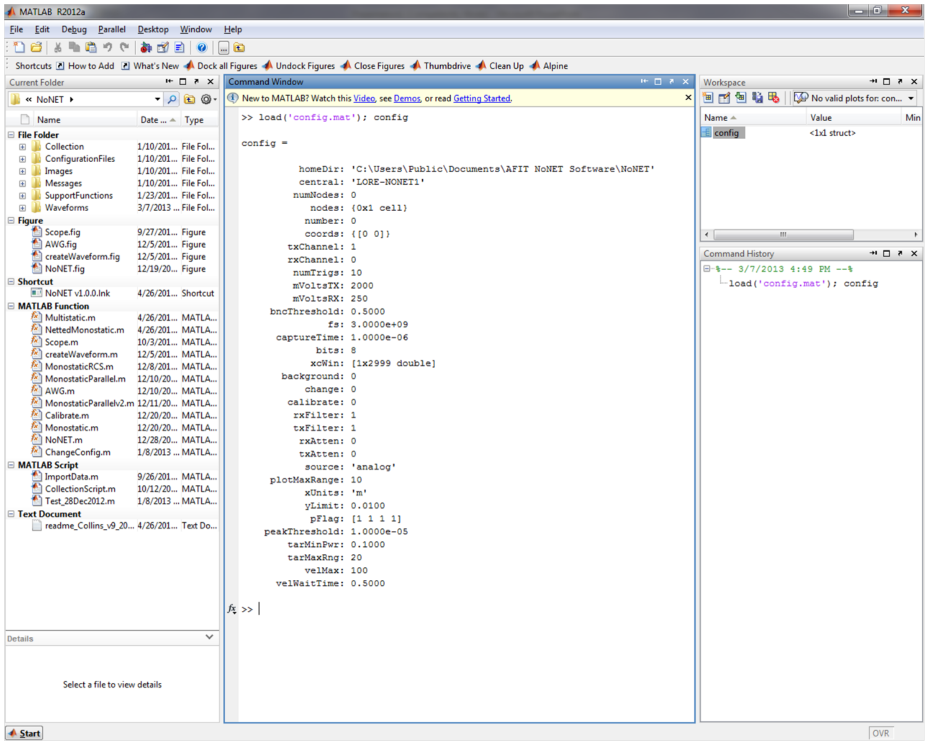

Figure C.13: Display configuration file from command line

the ConfigurationFiles folder, for use with all the NoNET functions. To change the configuration files back to the default configuration type "ChangeConfig('default')" into the matlab command prompt. Table C.1 displays each configuration setting and comments for that setting. Only the setting that are used for monostatic radar are included.

Table C.1: Configuration File Details

Configuration Field	Explaination
homeDir	home directory location
central	central node CPU name
txChannel	transmit channel on A/D board
rxChannel	receive channel on A/D board
numTrigs	number of collections to make on a single trigger command
mVoltsTX	peak to peak voltage for Tx channel in mV
mVoltsRX	peak to peak voltage for Rx channel in mV
bncThreshold	threshold of BNC trigger in V
fs	sampling frequency (see A/D card manual for acceptable frequencies)
captureTime	length in time for a single capture in S
bits	number of bits of A/D card
xcWin	correlation window index in samples
background	flag for background subtraction - DO NOT CHANGE
change	flag for change detection - DO NOT CHANGE
calibrate	samples shift from calibrate routine - DO NOT CHANGE
rxFilter	boolean selection of receive filter
txFilter	boolean selection of transmit filter
rxAtten	amount of receive attenuation in 0.5 dB steps from 0 to 31.5 dB
txAtten	amount of transmit attenuation in 0.5 dB steps from 0 to 31.5 dB
source	either ’analog’ or ’digital’
plotMaxRange	extent of plot range in meters or feet based on config.xUnits
xUnits	x-axis units either ’ft’ or ’m’
yLimit	y-axis upper limit in mW
pFlag	boolean vector for [Raw Xcorr, Raw Xcorr Peaks, Smoothed Xcorr, Target] plots
peakThreshold	min value to call a point a peak in mW

Once the user is satisfied with the configuration of the radar, the next step is to call the monostatic radar routine. This is done by typing "Monostatic(runtime, monotype)" where the **runtime** is the amount of time in seconds the radar will run for, and **monotype** is the digital signal processing that is done on the radar routine. Where the selections are **'raw'** uses the raw correlation results, **'change'** performs a change detection between collections, **'background'** performs a background subtraction. The background subtraction is the most useful and the most used mode of the AFIT RNR when performing monostatic radar.

C.5 NoNET Programming Tips

This section will cover a few programming tips for using matlab to interact with the AFIT RNR hardware. The three sections that will be discussed are the A/D converter, D/A converter, and the TTL card. Each piece of hardware interacts with matlab a little differently and can be a little difficult to comprehend at first. This section will provide some insight into the concepts that were learned during the course of the subject research.

C.5.1 A/D Converter.

The A/D converter (also called the capture card) drivers are provided in .NET code. Matlab uses .NET code fairly easily with little conversion necessary. The drivers for the capture card are loaded when matlab first starts up, with the function call "NET.addAssembly". To interact with the capture card matlab creates objects from the .NET drivers. To create the objects use the *Namespace.class* for the parameters you need to modify. The *Namespace* and *class* come from the ALNET2 Programming Manual found in "C:\Users\Public\Documents\AFIT NoNET Software\AL83xGT-E_DriversDisk_January2012\Docs" starting on page 30. Once the object is created fields and methods can be accessed using the convention *object.field* or *object.method()*. See the matlab code example below for usage within the NoNET InitializeBoard function:

```
%%%%%%%%%%%%%%%%%%%%%%%%%%%%%%%%%%%%%%%%%%%%%%%%%%%%%%%%%%%%%%%%%%%%%%

objBoard = nsAcqLog.nsAPI.AL8xGT(0,2,true);
objAcq = nsAcqLog.nsAPI.AcqParams_AL8xGT();
objCPTX = nsAcqLog.nsAPI.ChanParams_AL8xGT();
objCPRX = nsAcqLog.nsAPI.ChanParams_AL8xGT();

%%%%%%%%%%%%%%%%%%%%%%%%%%%%%%%%%%%%%%%%%%%%%%%%%%%%%%%%%%%%%%%%%%%%%%

objCPTX.InputRange.mV = config.mVoltsTX;
objCPRX.InputRange.mV = config.mVoltsRX;
Set(objAcq.ChanParams,config.txChannel,objCPTX);
Set(objAcq.ChanParams,config.rxChannel,objCPRX);
objAcq.NumberOfResultsToAverage = 0;
objAcq.SampleRate.Hz = config.fs;
objAcq.GateTree.Length.sec = config.captureTime;
if strcmp(MyRole,'central')
    objAcq.TriggerMode = nsAcqLog.nsAPI.eTriggerMode.Software;
elseif strcmp(MyRole,'node')
    objAcq.TriggerMode = nsAcqLog.nsAPI.eTriggerMode.BNC;
    objAcq.BNCThreshold.V = config.bncThreshold;
end
```

Use the Get() method to list all the settings of the current *namespace.class*. Use the Set() method to copy one object to another as seen in the above code snippet.

C.5.2 D/A Converter.

The D/A converter (also called the AWG or digital waveform generator) drivers are fairly straight forward. Unlike the capture card the drivers are not in .NET and require

the use of matlab's loadlibrary and calllib functions. The files to load and transmit a matlab array in a 32bit system are located in the SupportFunctions folder. To view the available functions to be called using the AWG drivers, load the driver using "loadlibrary('da12000_dll.dll', @da12000lib)" then type "libfunctionsview('da12000lib')". This will list all the available functions within that library to use within the calllib() function.

C.5.3 TTL Card.

The TTL card uses the drivers present in matlab. However a specific change needs to be made on computers that the NoNET has not been installed on before. To make this change first start at the matlab root directory then navigate to "toolbox\daq\daq\private" within that folder open the mwadvantech.ini file in wordpad and add the following to the end of the text file:

```
[PCI-1739U]
AIFifo=0
AIMaxSR=0
AIMinSR=0
AIDiffMult=0
AIInterruptMode=0
AIHwTrigger=0
AOMaxSR=0
AOMinSR=0
AOBipolar=0
DIOConfigWidth=48
DIOInputWidth=0
DIOOutputWidth=0
DIOPorts=6
SWInputType=1
```

Interaction with the TTL card through matlab is done entirely with the daq toolbox. The TTL card has 48 digital Inputs/Outputs (DIOs). The first 24 are taken up by the control for the switches and the attenuators. These 24 are pinned out according to Figure C.14. For programming examples see InitializeBoard, atten, or hwfilter functions in the SupportFunctions folder. The next 24 ports on the TTL card can be configured by software to be inputs or outputs. All these settings are done using the daq DIO toolbox.

Matlab DIO Line Number		Hardware Number	TTL Card Port Assignment	Pinout of Ribbon Cable to TTL Card Hookup		
24		A2 C2	PC 7	1	2	GND
23		A2 C8	PC6	3	4	GND
22		A2 C4	PC 5	5	6	GND
21	Tx Atten	A2 C16	PC 4	7	8	GND
20		A2 C0.5	PC 3	9	10	GND
19		A2 C1	PC 2	11	12	GND
18		A2 LE	PC 1	13	14	GND
17		A1 C2	PC 0	15	16	GND
16		A1 C8	PB 7	17	18	GND
15		A1 C4	PB 6	19	20	GND
14	Rx Atten	A1 C16	PB 5	21	22	GND
13		A1 C0.5	PB 4	23	24	GND
12		A1 C1	PB 3	25	26	GND
11		A1 LE	PB 2	27	28	GND
10	Source	SW 52	PB 1	29	30	GND
9	Select	SW 51	PB 0	31	32	GND
8		SW 42	PA 7	33	34	GND
7	Tx Filter	SW 41	PA 6	35	36	GND
6		SW 32	PA 5	37	38	GND
5		SW 31	PA 4	39	40	GND
4		SW 22	PA 3	41	42	GND
3	Rx Filter	SW 21	PA 2	43	44	GND
2		SW 12	PA 1	45	46	GND
1		SW 11	PA 0	47	48	GND
			+5V	49	50	GND

Figure C.14: NoNET TTL card pinout

Bibliography

[1] Addison, Paul S. *The Illustrated Wavelet Transform Handbook*. Institute of Physics Publishing, 2002.

[2] Baum, Carl E, Everett G Farr, et al. "Impulse radiating antennas". *Ultra-wideband, short-pulse electromagnetics*, 1:1993–139, 1993.

[3] ETS LINDGREN. *Double-ridged waveguide horn datasheet*, March 2007.

[4] Gardner, W.A. "Exploitation of spectral redundancy in cyclostationary signals". *Signal Processing Magazine, IEEE*, 8(2):14–36, April 1991. ISSN 1053-5888.

[5] Guosui, Liu, Gu Hong, and Su Weimin. "Development of random signal radars". *Aerospace and Electronic Systems, IEEE Transactions on*, 35(3):770–777, 1999.

[6] Horton, B.M. "Noise-Modulated Distance Measuring Systems". *Proceedings of the IRE*, 47(5):821 –828, may 1959. ISSN 0096-8390.

[7] Hughes, P.K. and J.Y. Choe. "Overview of advanced multifunction RF system (AMRFS)". *Phased Array Systems and Technology, 2000. Proceedings. 2000 IEEE International Conference on*, 21 –24. 2000.

[8] Kay, Steven M. *Intuitive probability and random processes using MATLAB*. Springer Science+Business Media, Inc., 2006.

[9] Knott, Eugene F. *Radar Cross Section Measurements*. SciTECH, 2006.

[10] Ludwig, M. *UHF Antenna Design for AFIT Random Noise Radar*. Master's thesis, Air Force Institute of Technology, 2012.

[11] Lukin, K. A. and R. M. Narayanan. "Fifty years of noise radar". *Physics and Engineering of Microwaves, Millimeter and Submillimeter Waves (MSMW), 2010 International Kharkov Symposium on*, 1–3. 2010.

[12] Mini-Circuits. *ZX76-31R5-PP+ Typical Performance Data*, February 2013. URL http://www.minicircuits.com/pages/s-params/ZX76-31R5-PP+_VIEW.pdf.

[13] Mini-Circuits. *ZX80-DR230+ Specification sheet*, February 2013. URL http://www.minicircuits.com/pdfs/ZX80-DR230+.pdf.

[14] Mini-Circuits. *ZX80-DR230+ Typical Performance Data*, February 2013. URL http://www.minicircuits.com/pages/s-params/ZX80-DR230+_VIEW.pdf.

[15] Mizui, K., M. Uchida, and M. Nakagawa. “Vehicle-to-vehicle communication and ranging system using spread spectrum technique (Proposal of Boomerang Transmission System)”. *Vehicular Technology Conference, 1993., 43rd IEEE*, 335 –338. may 1993. ISSN 1090-3038.

[16] Narayanan, R.M., X. Xu, and J.A. Henning. “Radar penetration imaging using ultra-wideband (UWB) random noise waveforms”. *Radar, Sonar and Navigation, IEE Proceedings*, 151(3):143 – 148, June 2004. ISSN 1350-2395.

[17] Nelms, M. E. *Development and evaluation of a multistatic ultrawideband random noise radar*. Master’s thesis, Air Force Institute of Technology, 2010.

[18] Pace, Phillip E. *Detection and Classifying Low Probability of Intercept Radar*. Artech House, 2009.

[19] Priestly, J. A. *AFIT NoNET Enhancements: Software Model Development and Optimization of Signal Processing Architecture*. Master’s thesis, Air Force Institute of Technology, 2011.

[20] Richards, Mark A., James A. Scheer, and William A. Holm (editors). *Principles of Modern Radar*. SciTECH publishing, Inc., 2010.

[21] Rossler, C.W., E. Ertin, and R.L. Moses. “A software defined radar system for joint communication and sensing”. *Radar Conference (RADAR), 2011 IEEE*, 1050 –1055. May 2011. ISSN 1097-5659.

[22] Schmitt, A. L. *Radar Imaging with a Network of Digital Noise Radar Systems*. Master’s thesis, Air Force Institute of Technology, 2009.

[23] Thorson, T. J. *Simultaneous range-velocity processing and SNR analysis of AFIT’s Random Noise Radar*. Master’s thesis, Air Force Institute of Technology, 2012.

[24] Turin, G. “An introduction to matched filters”. *Information Theory, IRE Transactions on*, 6(3):311–329, 1960. ID: 1.

REPORT DOCUMENTATION PAGE

Form Approved
OMB No. 0704-0188

1. REPORT DATE *(DD-MM-YYYY)*
21-03-2013

2. REPORT TYPE
Master's Thesis

3. DATES COVERED *(From - To)*
Oct 2011 - Mar 2013

4. TITLE AND SUBTITLE
Information Encoding on a Pseudo Random Noise Radar Waveform

5a. CONTRACT NUMBER

5b. GRANT NUMBER

5c. PROGRAM ELEMENT NUMBER

6. AUTHOR(S)
Hardin, Joshua A., Captain, USAF

5d. PROJECT NUMBER

5e. TASK NUMBER

5f. WORK UNIT NUMBER

7. PERFORMING ORGANIZATION NAME(S) AND ADDRESS(ES)
Air Force Institute of Technology
Graduate School of Engineering and Management (AFIT/EN)
2950 Hobson Way
WPAFB, OH 45433-7765

8. PERFORMING ORGANIZATION REPORT NUMBER
AFIT-ENG-13-M-22

9. SPONSORING / MONITORING AGENCY NAME(S) AND ADDRESS(ES)
Air Force Institute of Technology Attn: Dr. John Raquet
Advanced Navigation Technology (ANT) Center
2950 Hobson Way
WPAFB, OH 45433-7765

10. SPONSOR/MONITOR'S ACRONYM(S)

11. SPONSOR/MONITOR'S REPORT NUMBER(S)

12. DISTRIBUTION / AVAILABILITY STATEMENT
DISTRIBUTION STATEMENT A. APPROVED FOR PUBLIC RELEASE; DISTRIBUTION UNLIMITED

13. SUPPLEMENTARY NOTES

14. ABSTRACT
Navigation requires knowledge of current location and a planned destination. This is true with manned vehicles and unmanned vehicles. There are many ways to acquire the current location, including global positioning system (GPS), triangulation, radar, and dead reckoning. Today GPS is the most reliable and accurate navigation technique when there is a clear, unobstructed view of the satellite constellation. Various sensors can be used to perform indoor navigation; however, when the vehicle is autonomous the sensors need to provide the exact location to the system. This research determined if using a template replay strategy has the same RNR performance as using an analog noise source. Using the template replay approach, each RNR node has a priori knowledge about the transmitted waveforms of other nodes. The analysis here revealed that modifications do not significantly alter RNR functionality. The analysis revealed that even at SNIR equal to 0 dB, there are no parameters that can be reliably extracted other than transmitted signal bandwidth and transmitted template length; the transmitted message length was able to be extracted because the message was repeated over and over. If the message was not replayed the analysis showed that there would be no ability to extract parameters. Finally, by using the RNR to transmit digitally generated templates, digital communication is possible and the symbol error rate (SER) is traceable to simulated SER.

15. SUBJECT TERMS
Random Noise Radar; RNR; Template Replay; Simultaneous Communication and Radar

16. SECURITY CLASSIFICATION OF: a. REPORT	b. ABSTRACT	c. THIS PAGE	17. LIMITATION OF ABSTRACT	18. NUMBER OF PAGES	19a. NAME OF RESPONSIBLE PERSON
U	U	U	UU	118	Dr. Peter Collins (ENG)
					19b. TELEPHONE NUMBER *(include area code)* (937) 255-3636 x7256